Coordination Chemistry Reviews 256 (2012) 2453–2477

Contents lists available at SciVerse ScienceDirect

Coordination Chemistry Reviews

journal homepage: www.elsevier.com/locate/ccr

Review

Towards artificial photosynthesis: Supramolecular, donor–acceptor, porphyrin- and phthalocyanine/carbon nanostructure ensembles

Giovanni Bottari[a], Olga Trukhina[a], Mine Ince[a], Tomas Torres[a,b,*]

[a] Departamento de Química Orgánica, Facultad de Ciencias, Universidad Autónoma de Madrid, Cantoblanco, 28049 Madrid, Spain
[b] IMDEA-Nanociencia, c/ Faraday, 9, Cantoblanco, 28049 Madrid, Spain

Contents

ARTICLE INFO

Article history:
Received 10 January 2012
Accepted 12 March 2012
Available online 17 March 2012

Keywords:
Carbon nanotubes
Fullerene
Graphene
Molecular photovoltaics
Phthalocyanines
Porphyrins

ABSTRACT

The present review highlights the recent progresses in the preparation of supramolecular, donor–acceptor (D–A) porphyrin (Por)- and phthalocyanine (Pc)/carbon nanostructure systems assembled by using non-covalent interactions such as hydrogen bonding, metal–ligand, cation-crown ether or π–π interactions. The use of supramolecular interactions as a tool to promote the nanoscopic order of covalently-linked, Por- or Pc–C_{60} fullerene systems over large length scales will also be reviewed. The photophysical analysis of most of the D–A, supramolecular ensembles described will also be presented with the aim of rationalizing the effect on the photoinduced electron/energy-transfer dynamics of the structural and electronic features of these self-assembled systems and the recognition motif(s) used to self-assemble them. For some of the supramolecular systems reviewed, their incorporation as active components in photovoltaic devices will also be discussed.

Abbreviations: K_a, association constant; Bodipy, boron dipyrromethene; PCBM, 1-(3-carboxypropyl)-1-phenyl-[6,6]-C_{61}; CR, charge recombination; CS, charge separation; CT, charge transfer; CCG, chemically converted graphene; *o*-DCB, *ortho*-dichlorobenzene; DSC, differential scanning calorimetry; Fc, ferrocene; HOMO, highest occupied molecular orbital; Im, imidazole; IPCE, incident photon-to-current conversion efficiency; ITO, indium tin oxide; LUMO, lowest unoccupied molecular orbital; MWCNT, multi-walled carbon nanotube; NIR, near-infrared; Nc, naphthalocyanine; NG, natural graphite; 1-D, one-dimensional; PDI, perylenediimide; PET, photoinduced electron transfer; Pc, phthalocyanine; POM, polarized optical microscopy; PPV, poly(*p*-phenylene vinylene); Por, porphyrin; Py, pyrene; RGO, reduced graphene oxide; SMM, single-molecule magnet; SWCNT, single-walled carbon nanotube; SubPc, subphthalocyanine; THF, tetrahydrofuran; TTP, tetraphenylporphyrin; TEM, transmission electron microscopy; TPA, triphenylamine; XRD, X-ray diffraction; ZnONPs, zinc oxide nanoparticles.

* Corresponding author at: Departamento de Química Orgánica, Facultad de Ciencias, Universidad Autónoma de Madrid, Cantoblanco, 28049 Madrid, Spain. Tel.: +34 91 4974151; fax: +34 91 4973966.
E-mail address: tomas.torres@uam.es (T. Torres).

0010-8545/$ – see front matter © 2012 Elsevier B.V. All rights reserved.
doi:10.1016/j.ccr.2012.03.011

1. Introduction

The preparation and study of D–A hybrids involving porphyrinoids, like Pors [1] and Pcs [2], among other, and different allotropes of carbon such as C_{60} fullerene, carbon nanotubes or graphene [3], represents nowadays an important field of research.

The advantages of combining both types of structures are multiple. Pors and their synthetic analogues, Pcs, are thermally and chemically stable compounds which present a rich redox chemistry that can be easily tuned by the careful choice of the metal atom in the macrocycles' cavity and/or by placing adequate substituents at the macrocycles' peripheral and/or axial positions. Moreover, these compounds possess an intense optical absorption in the red/NIR of the solar spectrum [4], thus representing perfect light-harvesting systems and ideal components for photovoltaic devices [5]. The unique physicochemical properties of Pors and Pcs have prompted the incorporation of these macrocycles in a large number of D–A systems where their role is (i) to harvest light efficiently and (ii) once photoexcited, to act as an electron donor for an acceptor moiety [6].

Among the acceptor moieties employed for the preparation of Por- and Pc-based, D–A ensembles, members of the carbon nanostructures' family such as C_{60} fullerene, carbon nanotubes or graphene hold a privileged position. C_{60} fullerene possesses excellent electron acceptor properties, which coupled with its small reorganization energy (λ) [7], can give rise, when implemented in D–A systems, to the formation of very stable radical ion pair species [8]. Similarly to C_{60}, carbon nanotubes also present a high affinity for electrons which, once accepted, can be transported along their 1-D tubular structure [9]. For these reasons, both, fullerenes and carbon nanotubes are widely used as acceptor materials in organic and hybrid solar cells. More recently, graphene, one of the latest entries in the family of carbon nanostructures and one of the "rising stars" in the field of nanotechnology [10], has generated tremendous interest due to its extraordinary physical and mechanical properties which render it an outstanding material for electronics, material science and photoconversion systems [11].

Until now, a large variety of covalent and supramolecular systems based on Pors and/or Pcs and carbon nanostructures have been described and the photophysical properties of some of these D–A materials studied both in solution and/or in the solid state as well as their use as active components in photovoltaic devices [12,13]. When comparing these two constructing approaches (covalent vs. supramolecular), the use of supramolecular interactions for the preparation of systems based on Pors/Pcs and carbon nanostructures present some advantages over the covalent synthesis. This strategy, in fact, allows to obtain, in a convergent strategy, thermodynamically reversible assemblies of these functional entities, whose stability can be influenced by the careful choice of the supramolecular interaction(s) used as well as by some external conditions such as the temperature or the solvent polarity. In this context, the possibility to control the stability of such supramolecular ensembles could open up to possibility to influence/modulate some of the physical properties of these systems.

This review highlights recent progress in the preparation of supramolecular, D–A Por- and Pc/carbon nanostructure systems, assembled using noncovalent interactions such as hydrogen bonding, metal–ligand, cation-crown ether or π–π interactions. A section of this review will also be devoted to the use of supramolecular interactions as a tool to promote the nanoscopic order of covalently-linked, Por- or Pc–C_{60} systems over large length scales. The photophysical analysis of most of the D–A, supramolecular ensembles described will also be presented with the aim of rationalizing which effect the structural and electronic features of these self-assembled systems have on the photoinduced electron/energy-transfer dynamics. Special emphasis will be given to the occurrence of PET processes and the possibility to influence the lifetime of the resulting CS states as a function of the type of noncovalent interaction(s) used. For some of the supramolecular systems reviewed, their incorporation as active components in photovoltaic devices will also be presented.

2. Porphyrin- and phthalocyanine/C_{60} supramolecular systems

C_{60} fullerene is one of the acceptor units most employed for the preparation of noncovalent, D–A systems based on Pcs or Pors, due to its excellent electron affinity, which converts this spherical molecule in a perfect molecular component for the construction of photo- and electroactive systems. The extraordinary electron acceptor properties of C_{60} fullerene [8], coupled with its small reorganization energy (λ) and its ability for promoting ultrafast CS together with very slow CR features, have prompted the incorporation of this carbon nanomaterial in a large number of D–A supramolecular systems based on Pors and Pcs, where PET and solar energy conversion applications are sought [12b,12c,12d,12e,13].

In the following section, we will review some representative examples of such Por- and Pc/C_{60} supramolecular ensembles in which the two active units have been connected through hydrogen bonding interactions (Section 2.1), cation/crown ether interactions (Section 2.2) or via axial coordination of Pc or Por macrocycles to C_{60} fullerene covalently-functionalized with one or more coordinating ligands (Section 2.3).

Due to the limited length of this review, we have not included in this section any example of Por/C_{60} supramolecular complexes, cages or tweezers assembled using π–π supramolecular interactions as the "only" recognition motif [14] (*N. B.* to the best of our knowledge, no discrete Pc/C_{60} supramolecular complexes assembled using "exclusively" π–π supramolecular interactions have been reported to date).

2.1. Porphyrin- and phthalocyanine/C_{60} supramolecular systems assembled through hydrogen bonding interaction

The use of hydrogen bonding interactions represents an interesting "tool" for the preparation of biomimetic, D–A supramolecular systems based on Pors or Pcs. In such self-assembled architectures it is possible, by choosing the appropriate hydrogen bonding motif, to fine-tune the strength of the resulting supramolecular complex and ultimately to control the electronic coupling between the donor and acceptor moieties.

For example, directional, Watson-Crick hydrogen bonding interactions have been used as a recognition motif for the assembly of Pc/C_{60} (**1**) [15] or Por/C_{60} (**2**) [16] dyads (Fig. 1). These supramolecular systems have been prepared by complexation of a fulleropyrroline bearing a guanosine moiety (**3**) with cytidine-substituted Pc **4** (in the case of **1**) or Por **5** (in the case of **2**). In the case of **4**, UV/vis studies revealed that this molecule undergoes self-assembly as a result of both π–π interactions and cytidine–macrocycle interactions forming aggregates which can be disrupted upon addition of the guanosine-substituted fullerene derivative [17]. Fluorescence studies showed a nonlinear decrease of the fluorescence intensity of the cytidine-functionalized macrocycles **4** and **5** upon addition of fullerene derivative **3**, suggesting that photoinduced intracomplex CS takes place within ensembles **1** and **2**. Finally, transient absorption experiments on both ensembles revealed the formation of radical ion pair species with lifetimes of 2.02 μs (for **2** in dichloromethane) and 3.0 ns (for **1** in toluene). The significantly shortened charge-separated lifetime of **1** with respect to **2** is probably due to the pronounced coupling between the Zn(II)Pc macrocycle and C_{60} in **1**, as corroborated by the larger

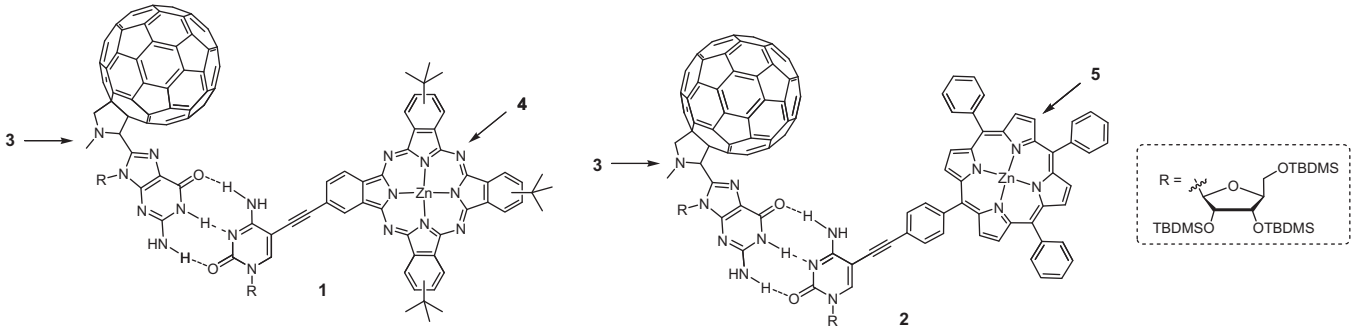

Fig. 1. Molecular structures of Pc/C_{60} (**1**) [15] and Por/C_{60} (**2**) [16] dyads assembled using Watson-Crick hydrogen bonding interactions.

K_a of this complex with respect to ensemble **2** (i.e., $2.6 \times 10^6\ M^{-1}$ vs. $5.1 \times 10^4\ M^{-1}$).

The PET properties of a Zn(II)Por_2/C_{60} supramolecular triad constituted by an uracil-substituted C_{60} assembled via a "three-point" hydrogen bonding to a diacetylamidopyridine spacer substituted at each end with a Zn(II)Por macrocycle have also been investigated [18]. Picosecond time-resolved emission and nanosecond transient absorption techniques were employed to characterize the photogenerated electron transfer products, revealing that, in such system, the relative position of the Por macrocycles with respect to the fullerene entity (i.e., near or far) influences the kinetics of the CS and CR events governed by a though-space electron transfer mechanism.

"Pure" through-bond electron transfer processes are often difficult to achieve in self-assembled D–A conjugates. In the large majority of these systems, in fact, through-space electron transfer mechanisms are also possible due to the flexible nature of the supramolecular ensembles which could lead to the spatial approximation of the donor and the acceptor moieties, leading, in turn, to important consequences on the overall electron transfer process both in terms of excited-state quenching and forward and back electron transfer dynamics. To solve this problem, rigid, self-assembled Por/C_{60} conjugates held together by complementary hydrogen bonding interactions have been prepared using an amidinium-carboxylate (**6**) [19] or a 2-aminopyridine-carboxylic acid (**7**) [20] hydrogen bonding motif (Fig. 2). In such dyads, the presence of "two-point" hydrogen bonds results in the formation of stable ensembles which, in the case of **6**, present a combination of hydrogen bonding and electrostatic interactions, can also self-assemble in highly polar solvents. Beside the formation of thermodynamically stable, D–A ensembles, the use of a "two-point" hydrogen bonding motif in **6** and **7** maintains the donor and the acceptor units at a fixed distance allowing to prepare ensembles which present reduced structural flexibility. In such systems, the two hydrogen bonds ensure an optimal pathway for the motion of charges and the electronic coupling between both electroactive units, thus maximizing the through-bond electron transfer dynamics. Detailed spectral and photochemical studies on Por/C_{60} dyads **6** and **7** revealed the formation of charge-separated species which are, generally, longer-lived (i.e., 10 μs in THF for **6** and 20–30 μs in *o*-DCB for **7**) with respect to their covalently-linked, Por–C_{60} counterparts.

A series of D–A, Por/C_{60} systems held together by Hamilton-receptor-based hydrogen bonding motif have been prepared through the complexation of either C_{60} derivatives containing cyanuric acid side chains to Hamilton-receptor substituted Pors [21] or Hamilton-receptor substituted C_{60} derivatives to Pors containing cyanuric acid side chains such as **8** (Fig. 3) [22]. Both ensembles, in which the Por and C_{60} components are connected by six hydrogen bonds, form stable 1:1 complexes with K_a as high as $10^5\ M^{-1}$ in toluene.

In the former paper [21], a detailed study on the nature of the Por macrocycle on the deactivation mechanism of the photoexcited state of these Por/C_{60} dyads was carried out revealing the occurrence of either electron (in the case of the Zn(II)Por-based dyad) or energy (in the case of the Sn(IV)Por-based dyad) transfer deactivation mechanisms, this latter process due to the shift of the Por oxidation potential caused by presence of Sn in the oxidation state of +4. In the latter report [22], the effect of the nature and length of the spacer between the fullerene and the cyanuric acid terminal unit on the stabilization of the photogenerated charge-separated species has been studied suggesting that spacers with good electron transfer properties such as *p*-phenylene-vinylene or fluorene (i.e., which have small attenuation factor (β) values [23]) facilitate electron transfer along the supramolecular bridge.

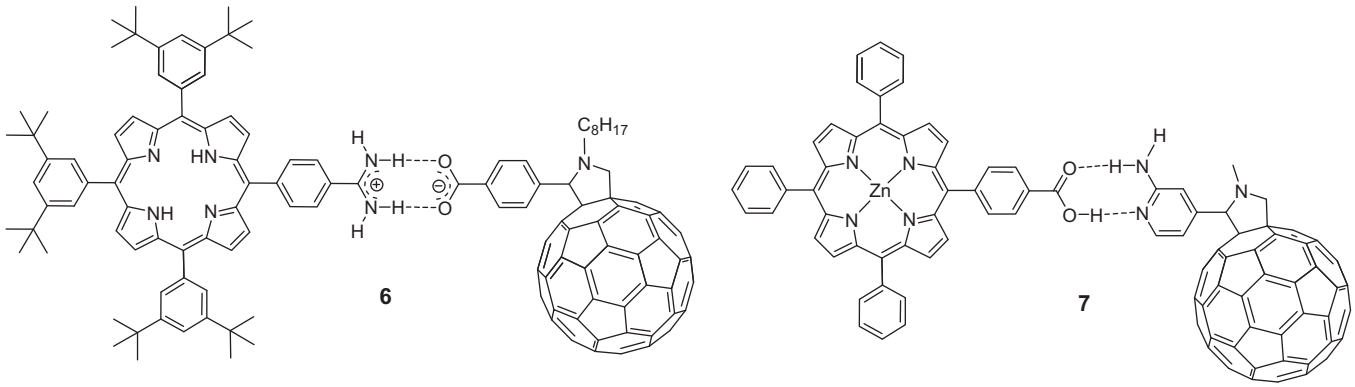

Fig. 2. Molecular structures of supramolecular Por/C_{60} dyads **6** [19] and **7** [20] assembled using amidinium-carboxylate (**6**) or 2-aminopyridine-carboxylic acid (**7**) hydrogen bonding interactions.

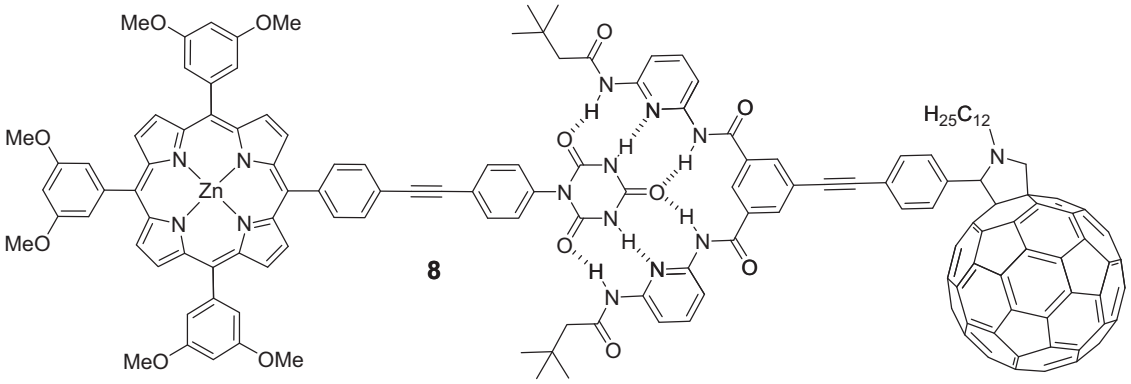

Fig. 3. Molecular structure of supramolecular Por/C_{60} dyad **8** assembled using a Hamilton-receptor-based hydrogen bonding motif [22].

More recently, a tricomponent supramolecular system (**9**) composed of a cyanuric acid-substituted Zn(II)Por macrocycle (**10**), a PDI unit bearing a Hamilton receptor (**11a** or **11b**), and a pyridine-substituted C_{60} (**12**) has been prepared by using two complementary supramolecular motifs, namely multipoint hydrogen bonding and metal–ligand complexation (Fig. 4) [24]. Ensemble **9** is a panchromatically absorbing system in which the Por and the PDI moieties present a complementary optical absorption. Photophysical studies have showed that, in the case of the supramolecular dyad Por **10**/PDI **11a**(**b**), upon selective photoexcitation of the PDI moiety, an energy-transfer process occurs from the singlet excited-state of the PDI to the Zn(II)Por macrocycle. On the other hand, pyridine-substituted C_{60} **12** and Zn(II)Por **10** associate via axial complexation, leading to D–A system **10**/**12**. Photophysical measurements confirm that, in supramolecular dyad **10**/**12**, an electron transfer process occurs from the singlet excited-state of Zn(II)Por **10** to the electron accepting fullerene **12**. In dyad **10**/**12**, the formed radical ion pair state decays with a lifetime of 1.0 ± 0.1 ns. Finally, time-resolved measurements on supramolecular PDI/Zn(II)Por/C_{60} triad **9** revealed that the initially occurring energy-transfer transduction from PDI **11a**(**b**) to Zn(II)Por **10** is followed by an electron transfer process from Zn(II)Por **10** to fullerene **12**. From multiwavelength analyses, the lifetime of the radical ion pair state in **9** – as a product of a cascade of light induced energy and electron transfer – was derived as 3.8 ± 0.2 ns.

2.2. Porphyrin- and phthalocyanine/C_{60} supramolecular systems assembled through cation/crown ether interaction

The association between cations (i.e., ammonium or alkali metal ions) and crown ether moieties has also been employed to construct D–A, Por- and Pc/C_{60} supramolecular ensembles, leading to systems which can be reversibly assembled/disassembled.

In 2002, the first report on a series of Pc/C_{60} fullerene pseudorotaxane systems assembled via alkylammonium/crown ether supramolecular interactions (**13a**–**c**) appeared (Fig. 5) [25]. The supramolecular complexes **13a**–**c** consists of a C_{60} derivative (**14**·PF_6^-) bearing a secondary dibenzylammonium moiety which is treaded into the dibenzo-24-crown-8 cavity of a Pc macrocycle (**15a**, **b** or **c**). The two components **14**·PF_6^- and **15a**, **b** or **c** self-assemble in chloroform solutions in a 1:1 stoichiometry and with a fairly high K_a ($1.53 \times 10^4\ M^{-1}$) as inferred by ^{1}H NMR experiments.

UV/vis titration experiments carried out in dichloromethane solutions of **15a** and an equimolar amount of the fullerene derivative **14**·PF_6^- failed to reveal any ground state electronic communication between the two active units. Similarly, electrochemical analysis on the fullerene reduction waves of derivative **14**·PF_6^- did not show substantial changes upon addition of Pc **15b**, thus suggesting that the formation of the supramolecular complex does not influence the reduction properties of the fullerene component. The lack of ground state electronic interactions between the

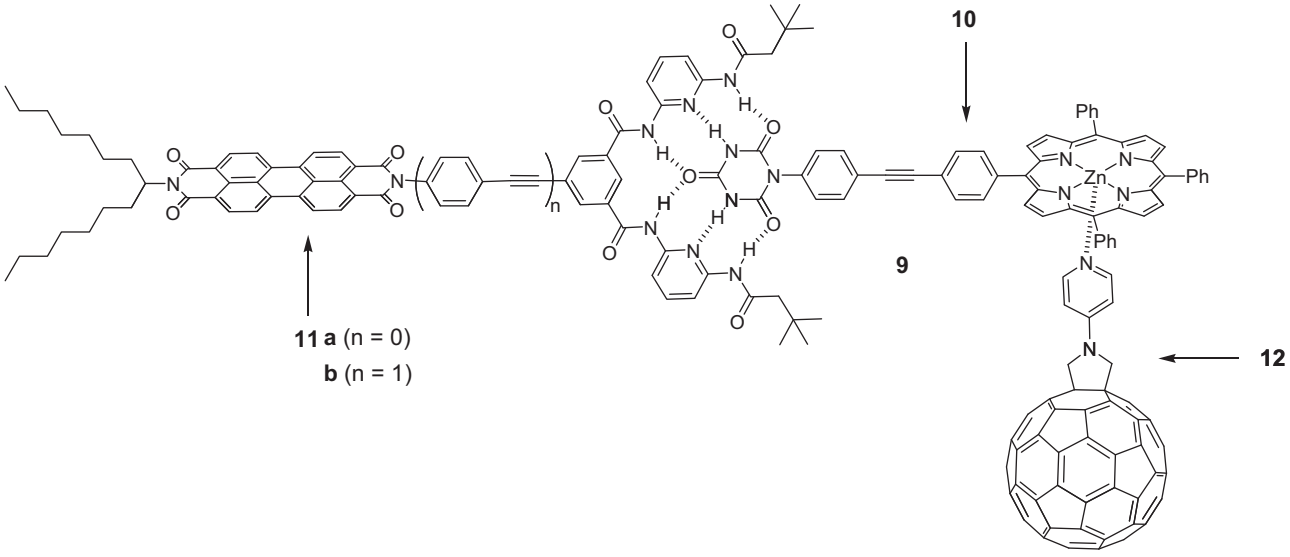

Fig. 4. Molecular structure of supramolecular PDI/Zn(II)Por/C_{60} triad **9** assembled using a Hamilton-receptor-based hydrogen bonding motif and metal–ligand complexation [24].

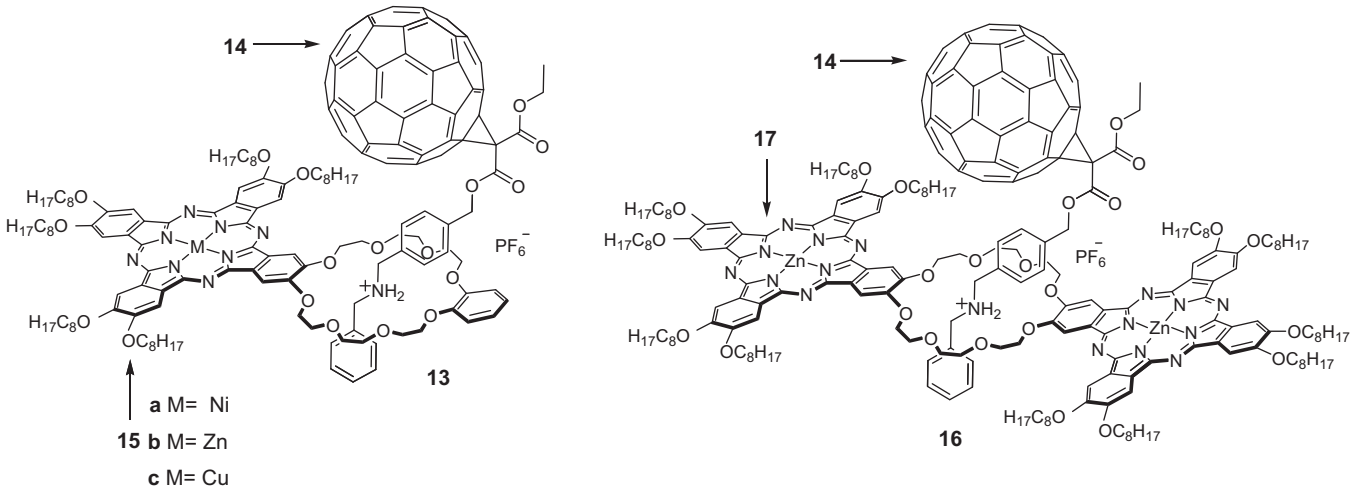

Fig. 5. Molecular structures of [2]pseudorotaxane Pc/C_{60} dyads **13a–c** [25] and Pc_2/C_{60} triad **16** [26].

two components in **13** could be due to the distance between the two electroactive units, which can adopt several conformations within the complex as revealed by molecular modeling studies.

With the aim of "forcing" the proximity between Pc and C_{60} while maintaining the same alkylammonium/crown ether recognition motif employed for the preparation of Pc/C_{60} dyads **13**, a Pc_2/C_{60} supramolecular triad (**16**) was prepared in which the number of Pc units around the crown ether macrocycle was increased from one (i.e., **15**) to two (i.e., **17**) (Fig. 5) [26]. Photophysical studies on **13** and **16** systems revealed, in both cases, a progressive, nonlinear quenching of the Zn(II)Pc fluorescence upon addition of the fullerene derivative **14**·PF_6^-. The fate of the photogenerated Pc excited-state was unveiled by transient absorption measurements which showed, for both **13** and **16**, the formation of microsecond-lived radical ion pair states (1.5 and 1.3 μs, respectively) as a result of an efficient *intra*complex electron transfer mechanism. It is worth mentioning that these supramolecular ensembles present a stabilization of more than two orders of magnitude of their radical ion pair state lifetimes with respect to covalently-linked Zn(II)Pc–C_{60} conjugates.

A Por/C_{60} system (**18**) has also been assembled through the complexation of crown ether-substituted Pors and a fullerene functionalized with an alkylammonium cation moiety (Fig. 6) [27]. In addition to the ammonium/crown ether interactions, intramolecular stacking of the C_{60} moiety and the Por unit has been put into evidence in **18** by ^{1}H NMR and UV/vis studies. Due to this additional recognition element, the K_a for complex **18** (i.e., $3.75 \times 10^5\ M^{-1}$) is increased by two orders of magnitude when compared to K_a values found for the complexation of the same ammonium-substituted fullerene with crown ether derivatives lacking the Por moiety.

The photophysical properties of a Por/C_{60} system (**19**) also assembled using alkylammonium/crown ether interactions have been investigated showing, for this system, reversible switching between intra- and intermolecular electron transfer dynamics in response to the presence or absence of potassium ions into the dyad solution, which ultimately controls the assembly/disassembly process of the supramolecular conjugate **19** (Fig. 7) [28].

Similarly, a Zn(II)Por/C_{60} supramolecular dyad (**20**) assembled by a using a combination of alkylammonium cation/crown ether interactions and zinc-pyridine metal–ligand axial coordination, the so-called "two-point" binding strategy, has also been prepared (Fig. 7) [29,30]. Photophysical studies on this system revealed the occurrence of light induced electron transfer from the singlet excited Por macrocycle to the fullerene moiety, with a lifetime for the photogenerated CS state (i.e., 210 ns) which could be increased by attenuating the π–π interactions by the addition of pyridine to the solution containing dyad **20** (i.e., 500 ns). This latter observation could be attributed to the increased distance between the Por and the fullerene entities as a result of

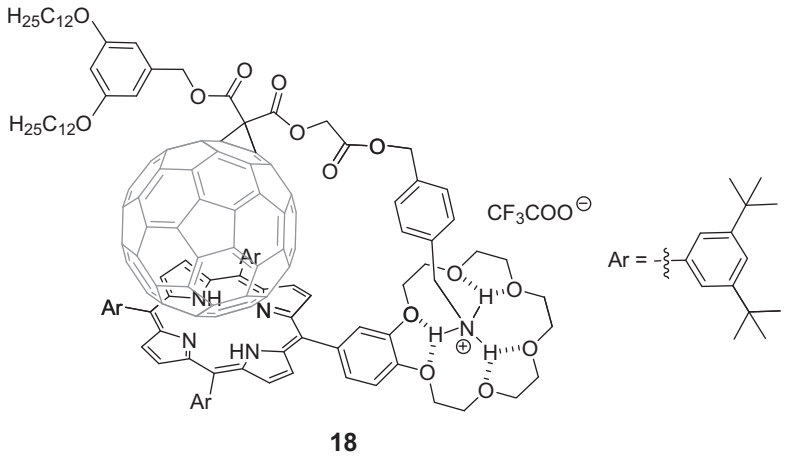

Fig. 6. Supramolecular Por/C_{60} hybrid **18** presenting crown ether inclusion and π–π stacking binding motifs [27].

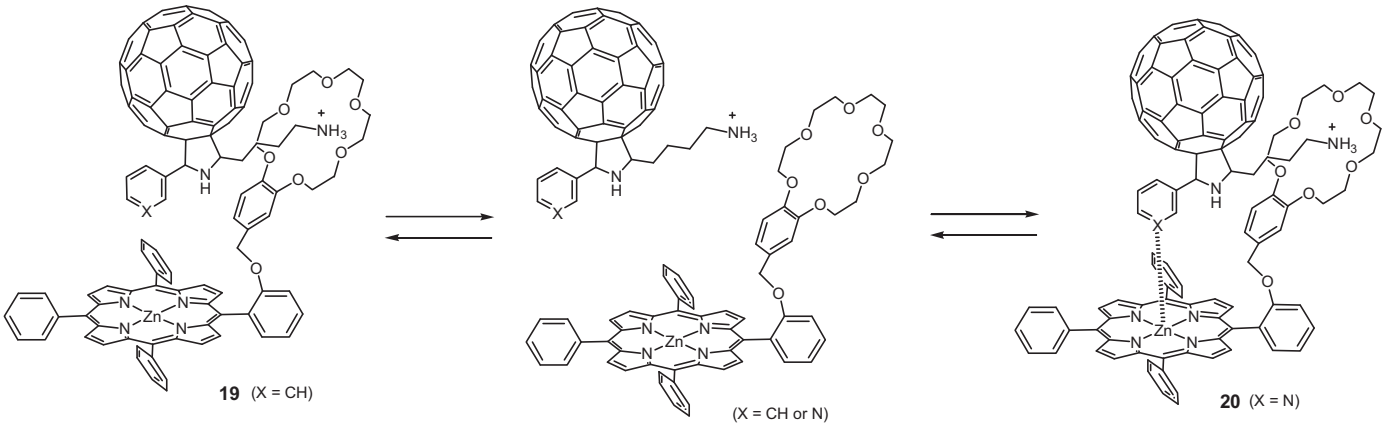

Fig. 7. Supramolecular Por/C_{60} hybrids presenting a crown ether inclusion binding motif (**19**) [28] and a combination of metal–ligand axial coordination and crown ether inclusion binding motifs (**20**) [29,30].

the coordination of the unsubstituted pyridine which displaces the C_{60}-substituted pyridine from its coordination to the zinc atom.

PET processes were also observed in Zn(II)Por systems doubly functionalized with crown ether moieties and self-assembled using a "two-point" binding strategy with fullerene functionalized with pyridine or alkylammonium cation entities leading to 1:2 Por/$(C_{60})_2$ ensembles [31]. A comparison of the rates of the CS of this Por/$(C_{60})_2$ ensemble with a similar 1:1 Por/C_{60} supramolecular system also assembled using a "two-point" binding strategy suggests that employing a higher number of acceptor entities improves the electron transfer rates.

More complex, supramolecular ensembles constituted of two fullerene derivatives containing both a pyridine and a terminal ammonium moiety and two crown ether-containing Zn(II)Pcs (**21**) [32] or Zn(II)Pors (**22**) [33] have also been prepared (Fig. 8).

The assembly strategy which leads to the formation of these tetrads is based on the K^+-induced, cofacial stacking of the two macrocycles and the "two-point" binding of the fullerene derivatives to the Pc or Por macrocycle through both metal–ligand axial coordination and ammonium/crown ether complexation.

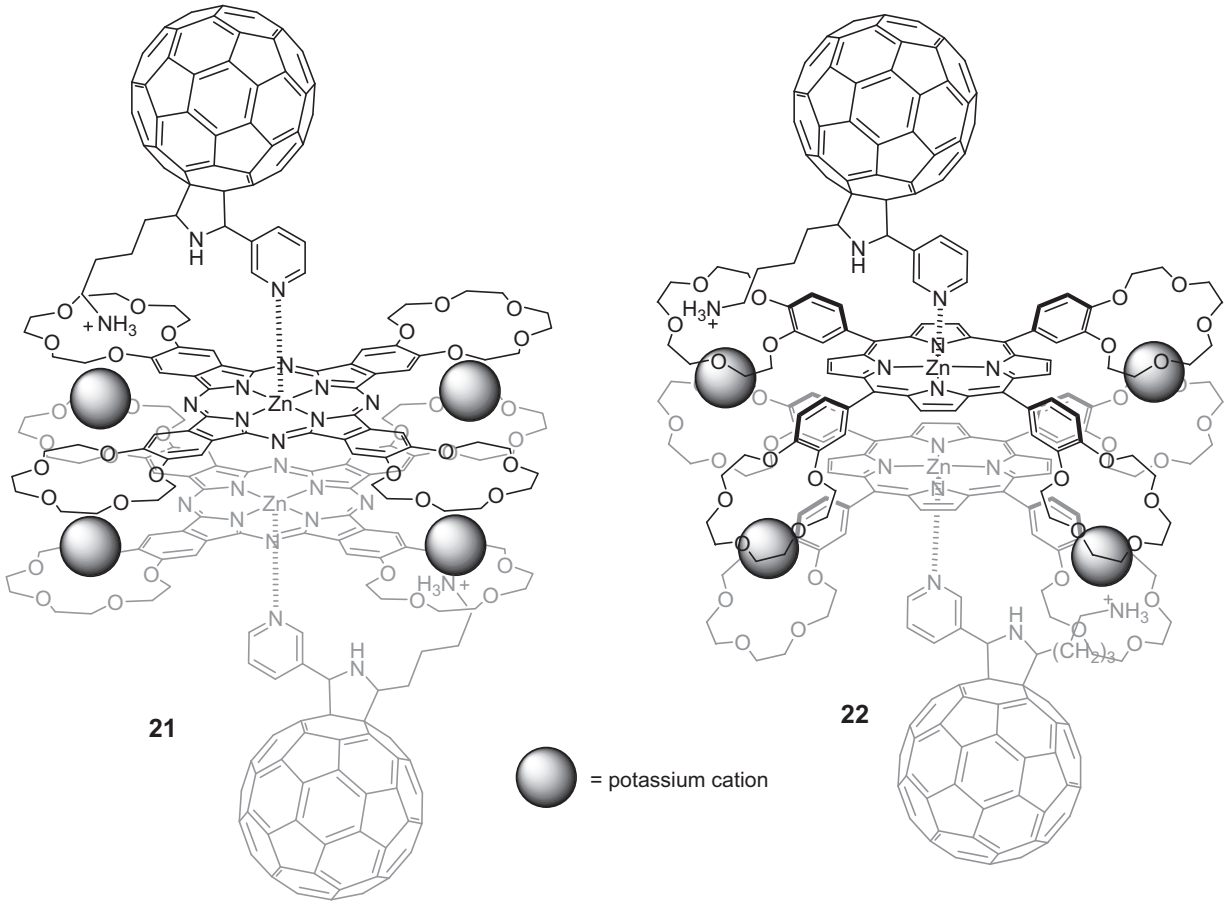

Fig. 8. Molecular structures of Zn(II)Pc_2/$(C_{60})_2$ **21** [32] and Zn(II)Por_2/$(C_{60})_2$ **22** [33] supramolecular ensembles.

Both supramolecular tetrads exhibit enhanced electron transfer properties as inferred by the formation of a charge-separated state. However, whereas in the case of the Por ensemble **22** the electron transfer to the fullerene entity occurs from the singlet excited Zn(II)Por stacked dimer, on the other hand in the case of **21** the radical ion pair product is due to electron injection of the triplet excited-state of the Zn(II)Pc stacked dimer to C_{60}. In this latter system, the cofacial Pc–Pc stacking plays an important role in stabilizing the charge-separated state leading to a lifetime of the radical ion pair of 6.7 μs, a lifetime significantly longer than the value reported for **22** (i.e., 50 ns). The significant increase in the lifetime of the CS state in **21** with respect to **22** may result from the smaller reorganization energy of the electron transfer dynamics for the more π-expanded Pc macrocycle relative to the Por one.

The supramolecular interactions between a Zn(II)Pc [34] or a Zn(II)Por [29] macrocycle bearing four crown ether moieties and two structurally related fulleropyrrolidine derivatives functionalized with an alkylammonium pendant unit have also been investigated. The presence of several crown ether binding sites at the macrocycles' periphery results in the formation of D–A supramolecular conjugates in which multifullerene species are in close proximity to the Pc or Por units. Photochemical and photophysical studies involving steady-state and time-resolved fluorescence measurements as well as transient absorption techniques were carried out on both the Por- and Pc/multifullerene ensembles revealing, in both cases, the occurrence of PET from the singlet excited-state of the macrocycle to the fullerene unit. The evaluated lifetimes of the radical ion pairs for the Zn(II)Pc/multifullerene conjugates were hundreds of nanoseconds (i.e., 290 ns) and are much longer compared to the Zn(II)Por/multifullerene analogues (i.e., 80 ns), probably due to a combination of electronic and topological features.

2.3. Porphyrin- and phthalocyanine/C_{60} supramolecular systems assembled via metal–ligand axial coordination

During the past few decades, metal-directed self-assembly has become an important tool used by chemists to prepare large and elaborate complex ensembles from structurally simpler components. Moreover, these self-assembled supramolecular architectures often present large K_a's, approaching, in some cases, the stabilities observed for the covalent systems.

In this context, several examples of self-assembled, supramolecular D–A systems based on C_{60} fullerene functionalized with pyridine or Im moieties complexing a central metal (zinc, magnesium, or ruthenium) of macrocyclic compounds such as Pors, Pcs or Ncs have been synthesized and studied [12b,12c,12d,12e].

Supramolecular ensemble **23a** constituted by a pyridine-appended C_{60} and Zn(II)TTP was among the first reported Por-based, D–A system assembled via metal–ligand coordination interaction (Fig. 9) [35]. The UV/vis and ^{1}H NMR spectral studies carried out on this system revealed the formation of a 1:1 complex between the donor and acceptor entities. Fluorescence studies showed an efficient quenching of the Zn(II)Por emission upon axial coordination of the pyridine-substituted C_{60}, whereas free-energy calculations suggested the possibility for a PET process from the singlet excited zinc tetrapyrrole moiety to C_{60}. Analysis of the monoexponential fluorescence decay of ensemble **23a** upon addition of the pyridine-substituted C_{60} allowed to estimate the rate of the electron transfer process which was $(2.4 \pm 0.3) \times 10^8\ s^{-1}$.

The previous study has been completed by preparing a series of Por/C_{60} systems **23b–d** in which the nature of the ligand has been varied (i.e., pyridine for **23a–c** and Im for **23d**) as well as the relative spatial orientation of the Por and C_{60} units within the Por/C_{60} ensemble (i.e., using fulleropyrrolidine derivatives bearing an *o*- (**23b**), *m*- (**23a**) or *p*-pyridine (**23c**) ligand) to investigate how these

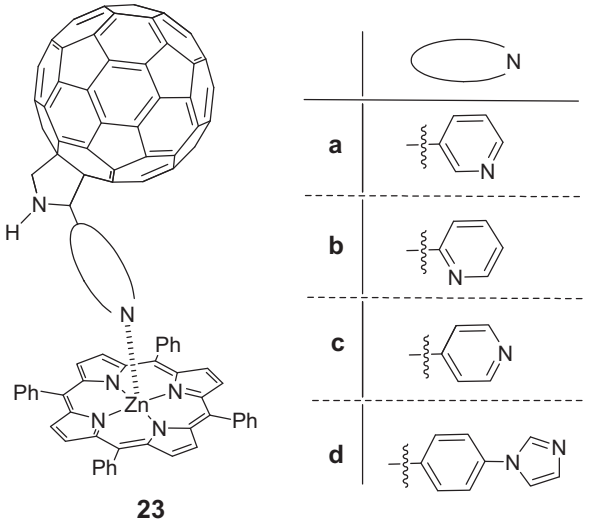

Fig. 9. Structures of supramolecular Zn(II)TTP/C_{60} ensembles **23a–d** [35,36].

changes would affect the communication between the donor and the acceptor units (Fig. 9) [36].

For all these compounds, UV/vis, ^{1}H NMR, mass spectrometry and computational studies revealed a 1:1 assembly stoichiometry. The determined K_a of these complexes followed the order *o*-pyridyl < *m*-pyridyl ≈ *p*-pyridyl << *N*-phenyl Im. Ab initio B3LYP/3-21G(*) methods were used to determine the geometric and electronic structures of the dyads, demonstrating that the majority of the HOMO was located on the Zn(II)TPP unit, while the LUMO was entirely located on the fullerene moiety. Electrochemical studies showed weak interactions between the donor and the acceptor components in the ground state. On the other hand, photophysical studies (i.e., steady-state and time-resolved emission as well as transient absorption measurements) demonstrated significant interactions between the two entities. In *o*-DCB, the main quenching pathway for the **23a–d** systems involved CS from the singlet excited Zn(II)TPP to C_{60}. On the contrary, in a coordinating solvent like benzonitrile, intermolecular electron transfer takes place mainly from the triplet excited Zn(II)TPP macrocycle to C_{60}, thus suggesting that, for such systems, the deactivation pathway is strongly dependent to the solvent media. In the case of the Zn(II)TPP/**23c** complex, long charge-separated lifetimes were observed in polar solvents like THF (~10 μs) or benzonitrile (several hundreds of microseconds) [37].

In the previous systems, both through-space and through-bond communication is possible between the Por and the C_{60} moieties. In order to reduce the through-space deactivation channel to a minimum, a Por/C_{60} ensemble (**24**) was prepared in which a pyridine unit was appended to the nitrogen of the fulleropyrrolidine (**12**) (Fig. 10) [38]. In such ensemble, in fact, the linear geometry

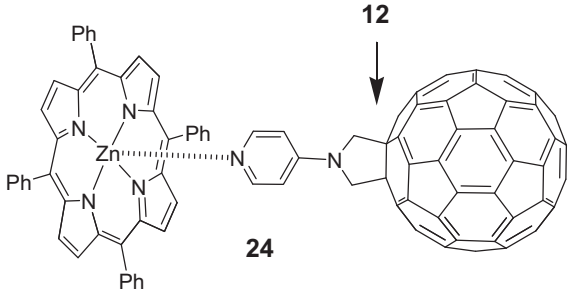

Fig. 10. Molecular structure of Zn(II)TTP/C_{60} supramolecular ensemble **24** [38].

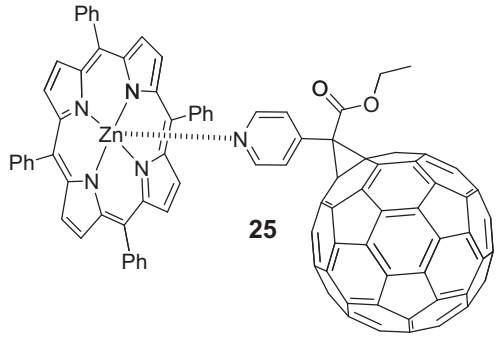

Fig. 11. Molecular structure of Zn(II)TTP/C_{60} supramolecular ensemble **25** [39].

presented by dyad **24** hampers any through-space communication between the Por and C_{60}. The K_a for such Por/C_{60} supramolecular complex was obtained from fluorescence titration experiments in *o*-DCB, giving a value of $7.4 \times 10^4\ M^{-1}$, which was five times smaller than the one of **23c** in the same solvent. These results indicate that the substitution pattern of the fulleropyrrolidine entity considerably affects the binding strength of the resulting Por/C_{60} dyad, being a parameter that one could use in order to optimize the electron- and energy-transfer dynamics in such supramolecular systems. Electrochemical measurements showed a 40 mV positive shift of the first one-electron reduction of the C_{60} moiety upon complexation to Zn(II)TPP, thus suggesting the occurrence of a ground state electronic interaction between the Zn(II)TPP macrocycle and C_{60}.

A methanofullerene derivative obtained by Bingel-Hirsch reaction and bearing a pyridine residue at the methano bridge has also been complexed to Zn(II)TTP via metal–ligand interaction leading to supramolecular ensemble **25** (Fig. 11) [39]. The K_a of the Zn(II)TPP and C_{60} components in the 1:1 Zn(II)TTP/C_{60} complex was $(3.6 \pm 0.15) \times 10^3\ M^{-1}$ in C_6D_6 solution as determined by ^{1}H NMR titration, and $(3.0 \pm 0.4) \times 10^3\ M^{-1}$ as determined by fluorescence titrations in toluene. Extremely fast, luminescence quenching of the Zn(II)TPP moiety was recorded for complex **25** by time-resolved luminescence spectroscopy and was attributed to efficient energy transfer from the Por to the C_{60} unit.

A supramolecular system based on tetra-*tert*-butyl Zn(II)Pc and a pyridine-appended fulleropyrrolidine has also been prepared (**26**) and the photophysical properties of the resulting ensemble studied (Fig. 12) [26]. The coordination constant for this Pc/C_{60} complex was $4.8 \times 10^3\ M^{-1}$. The weak K_a of the complex facilitates, after photoexcitation of the dyad and rapid intramolecular electron transfer, the crucial break-up of the radical pair Zn(II)Pc$^{\bullet+}$/pyridine-substituted $C_{60}^{\bullet-}$ species into the free radical ions, Zn(II)Pc$^{\bullet+}$ and pyridine-substituted $C_{60}^{\bullet-}$, the lifetime of this radical pair species being governed by a nearly diffusion controlled, intermolecular back electron transfer. By contrast, the much stronger binding typical of Pc–C_{60} covalent systems prevents this splitting and, hereby, shortens the radical pair lifetime to the nanoseconds time regime.

A stronger binding was observed for system **27** consisting in an Im-substituted fulleropyrrolidine axially coordinated to a Zn(II)Nc (Fig. 12) [40]. Zn(II)Nc was chosen as a sensitizer to extend the absorption properties of the resulting dyad, whereas Im-appended fullerene, which present a higher basicity than its pyridine-functionalized analogue, provided stronger binding between the two entities. The K_a of Zn(II)Nc/C_{60} dyad **27** was $6.2 \times 10^4\ M^{-1}$ in toluene that is an order of magnitude higher than the values for Zn(II)TPP/C_{60} **23d** or Zn(II)Pc/C_{60} **26**. Picosecond transient absorption measurements on **27** revealed the formation of the radical pair Zn(II)Nc$^{\bullet+}$/$C_{60}^{\bullet-}$, which presented rates of CS and quantum yields of $1.4 \times 10^{10}\ s^{-1}$ and 0.97 in toluene and $8.9 \times 10^9\ s^{-1}$ and 0.96 in *o*-DCB, respectively.

Ncs were also complexed with a series of pyridine-appended fulleropyrrolidines (**28**, **29** [41] and **30** [42]) bearing a secondary electron-donor moiety (Fc, *N*,*N*-diaminophenyl or pyridine, respectively) (Fig. 13). The binding constants of these systems were $7.4 \times 10^4\ M^{-1}$ for Zn(II)Nc/**28** and $10.2 \times 10^4\ M^{-1}$ for Zn(II)Nc/**29** in *o*-DCB, that is slightly higher than that of Zn(II)Nc/C_{60} **27** (i.e., $6.2 \times 10^4\ M^{-1}$). These binding constant values suggest, considering that the Im ligand binds strongly to the Zn(II)Nc (vide supra), that the incorporation of a second electron donor on the pyrrolidine unit increases the basicity of the pyridyl group which, in turn, facilitates the axial coordination of the fullerene derivative. In these triads, photoexcitation of the Zn(II)Nc entity gave rise to an efficient electron transfer process from the Nc macrocycle to C_{60} resulting in the formation of radical ion pair species with a lifetime of 10–15 ns.

One or two secondary Fc, electron-donor units have also been covalently-connected at the periphery of a Zn(II)Por macrocycle which has then been complexed to either a pyridine- or Im-appended fulleropyrrolidine leading to ensembles **31** (Fig. 14) [43]. In the case of the Zn(II)Por-Fc$_n$ (n = 1 or 2) systems, upon photoexcitation, efficient electron transfer from the Fc to the singlet excited Zn(II)Por occurred depending upon the nature of the spacer, resulting in the formation of a Fc$^{\bullet+}$–Zn(II)Por$^{\bullet-}$ radical pair species. On

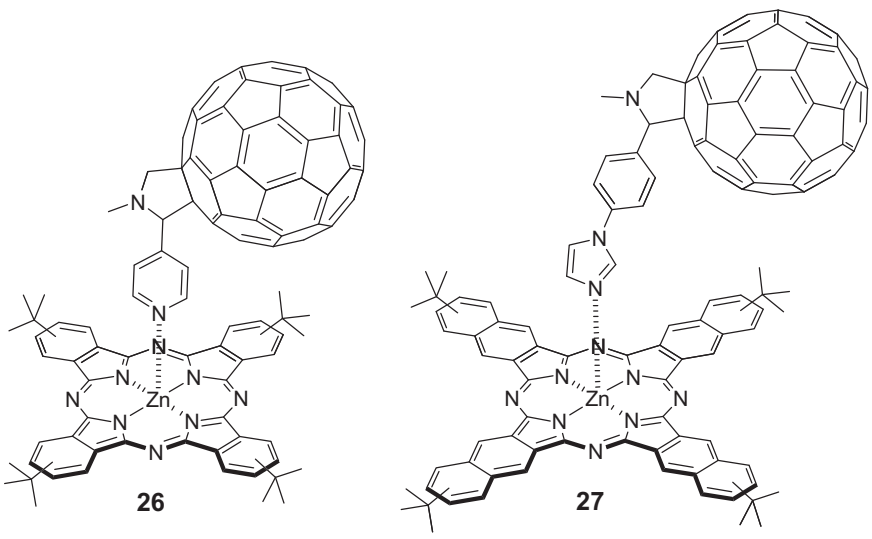

Fig. 12. Molecular structures of Zn(II)Pc/pyridine-substituted C_{60} **26** [26] and Zn(II)Nc/Im-substituted C_{60} **27** [40].

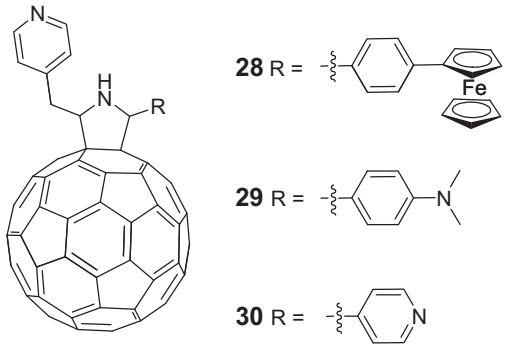

Fig. 13. Structures of pyridine-appended C_{60} derivatives **28–30** [41,42].

the other hand, upon axial coordination of the fulleropyrrolidines to the Zn(II)Por-Fc_n (n = 1 or 2) system, the formation of a CS state $Fc^{\bullet+}$–Zn(II)Por/$C_{60}^{\bullet-}$ was observed, which proved to be longer-lived with respect to the uncomplexed Zn(II)Por-Fc_n (n = 1 or 2) systems.

Fullerene **30** bearing two pyridine entities was also used in order to complex a covalent Zn(II)Por dimer forming a stable 1:1 complex ($K_a = 1.8 \times 10^5\ M^{-2}$) [44]. The large binding constant observed for the coordination of the C_{60} bipyridine to the Zn(II)Por dimer is probably due to the proximity effect of the two Por macrocycles. Nanosecond transient absorption studies on such supramolecular complex revealed the occurrence of a charge-separated quenching pathway with a rate of the CR process of $\sim 2 \times 10^8\ s^{-1}$ at room temperature in *o*-DCB.

Ru(II)Pcs have also been used in order to prepare Pc/C_{60} supramolecular systems, since they can form stable supramolecular architectures through metal–ligand coordination of, for example, pyridine derivatives which can complex either to one or both faces of the macrocycle. These features have been exploited to construct a series of Ru(II)Pc/C_{60} hybrids (**32**–**34**) bearing an orthogonal geometry [45] (Fig. 15). Starting from the tetra-*tert*-butylated phthalocyaninato Ru(II) derivative having a strongly ligating axial carbonyl moiety at one of the two axial Ru(II) coordination sites, dyad **32** and triad **34** were prepared by treatment with monopyridyl-functionalized C_{60} ligand **12** (in order to obtain dyad **32**) or with a highly elaborated fulleropyrrolidine ligand bearing two pyridine units in a *trans*-1 relative arrangement (in order to obtain triad **34**). Triad **33** was prepared in a similar manner from the monopyridyl-functionalized C_{60} ligand **12** and the tetra-*tert*-butylated phthalocyaninato ruthenium(II) derivative having two labile, benzonitrile molecules at its axial positions. Electrochemical experiments on arrays **32**–**34** showed electronic coupling between the two electroactive components in the ground state. From the photophysical point of view, the use of Ru(II)Pcs rather than Zn(II)Pcs, which present a high-lying triplet excited-state, represents a real benefit. In such systems, in fact, the energy-wasting and unwanted CR has been successfully reduced by pushing it far into the Marcus inverted region [7], with radical ion pair state lifetimes on the order of hundreds of nanoseconds for the monopyridine-substituted C_{60} adducts (i.e., **32** and **33**). On the other hand, in triad **34**, which presents a unique hexakis-C_{60} functionalization, a cathodic shift of the reduction potential is observed, which in turn raises the radical ion pair state energy. Nevertheless, the energy of the triplet excited-state localized on the Ru(II)Pc is not high enough, thus offering a rapid deactivation of the radical ion pair state.

Similarly that in the case of Pcs, ruthenium has also been used as metal atom in Por/C_{60} ensembles such as in the case of the Ru(II)TTP/**23c** supramolecular dyad in which intramolecular energy transfer has been observed from the photoexcited Ru(II)Por unit to the fullerene moiety in toluene. On the other hand, weak intramolecular electron transfer was occurring in a more polar solvent like benzonitrile [37].

A structurally more complex, supramolecular D–A ensemble (**35**) has also been reported (Fig. 16) [46]. Triad **35** is composed of a C_{60} fullerene electron acceptor and two Fc electron-donor units coupled by hydrogen bonds in a rotaxane architecture. Additionally, **35** presents a Ru(II)TPP(CO) macrocycle coordinated to a pending pyridyl group present on the fulleropyrrolidine moiety. In such system, the alignment of the photo/electroactive units along a supramolecular electrochemical gradient promotes a unidirectional cascade of two consecutive through-space CT processes between the three components (i.e., initial formation of the $Por^{\bullet+}/C_{60}^{\bullet-}$-$Fc_2$ species followed by a CT shift reaction leading to the Por/$C_{60}^{\bullet-}$-$Fc_2^{\bullet+}$ species). Interestingly, the lifetime of the final CT product of **35** was longer than that of a system analogous to **35** lacking the Fc-substituted macrocycle.

A Mg(II)TTP/C_{60} supramolecular systems assembled by metal–ligand axial coordination of Im-substituted C_{60} to a Mg(II)TTP macrocycle have also been reported [47]. Spectroscopic studies on such system revealed the formation of a 1:1 Mg(II)TTP/C_{60} supramolecular complex with a K_a

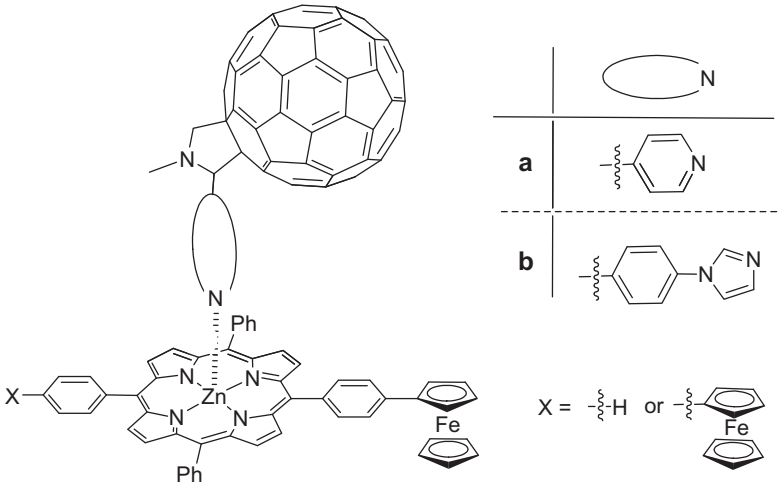

31

Fig. 14. Structures of supramolecular ensembles **31** [43].

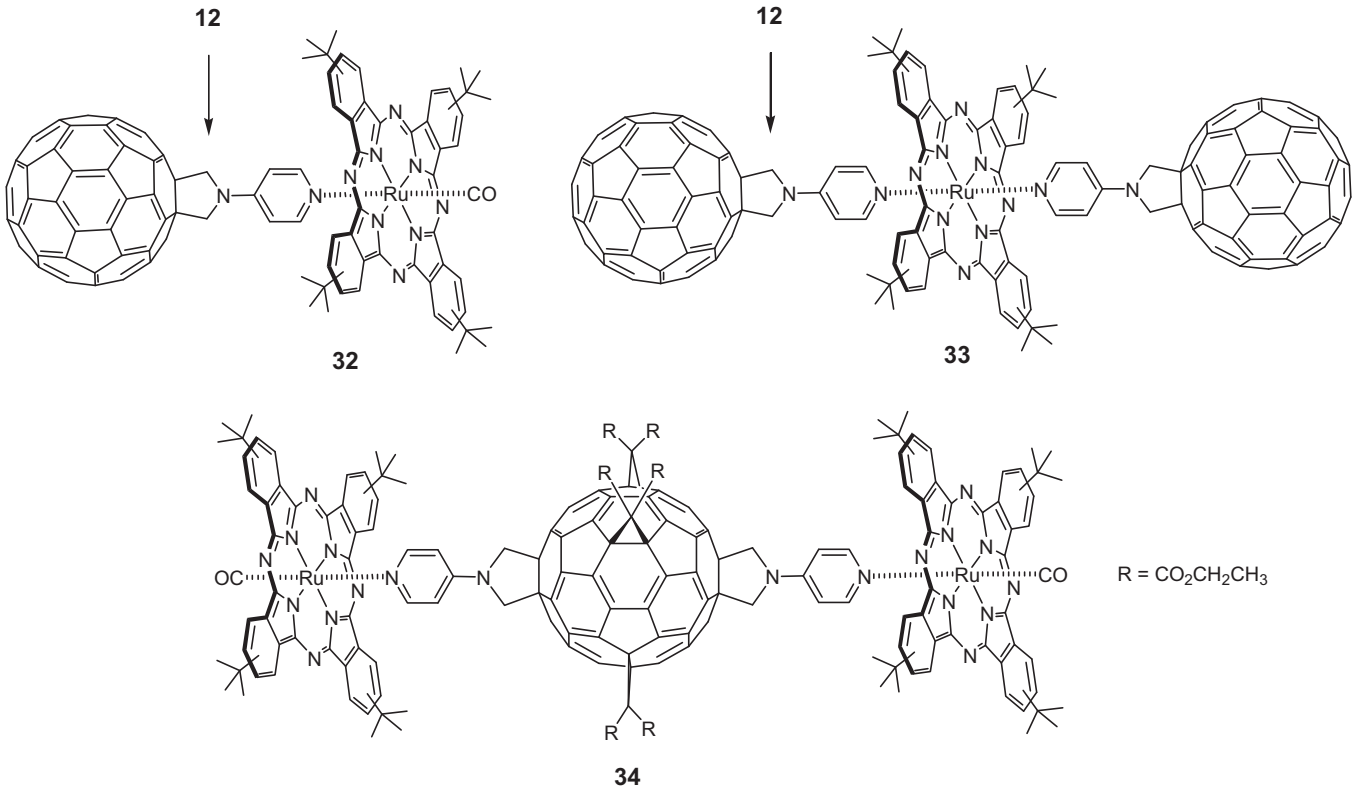

Fig. 15. Structures of the supramolecular Ru(II)Pc/C_{60} dyad **32** and triads **33** and **34** [45].

of $(1.5 \pm 0.3) \times 10^4\ M^{-1}$. The excited-state features of the Mg(II)TTP/C_{60} ensemble were monitored by steady-state and time-resolved emission as well as transient absorption techniques, suggesting the occurrence of a fast and efficient PET process leading to the formation of a Mg(II)$TTP^{\bullet+}$/$C_{60}^{\bullet-}$ species.

Catechol ligands have also been used in order to prepare a Pc/C_{60} supramolecular complex in which a catechol-functionalized C_{60} fullerene was axially coordinated to a titanium(IV)Pc [48]. Photophysical studies on such complex demonstrated the occurrence of PET from the photoexcited Pc to the fullerene unit.

The stability of the charge-separated state in Por/C_{60} dyads can be fine-tuned by varying the distance between the donor and the acceptor moieties, by increasing the donor strength of the Por macrocycle, or by enhancing the acceptor features of the fullerene moiety [49]. This last approach has been employed for the construction of a D–A dyad (**36**) with improved properties, containing $C_{59}N$ heterofullerene instead of C_{60} (Fig. 17). The supramolecular dyad **36**, which possesses a quasi-linear geometry, involves a heterofullerene acceptor and a Zn(II)Por donor connected via metal–ligand coordination [50].

The fluorescence quenching of Zn(II)Por upon addition of the heterofullerene as well as the decreasing of its fluorescence lifetime (0.003) was consistent with the occurrence of a static quenching event. The K_a for complex **36** was $(9.5 \pm 0.3) \times 10^3\ M^{-1}$ in toluene, and $(1.17 \pm 0.7) \times 10^4\ M^{-1}$ in *o*-DCB that is comparatively

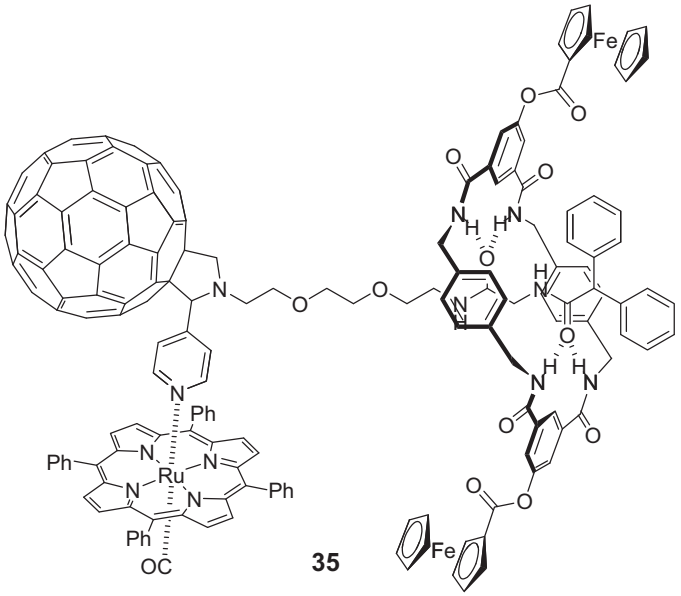

Fig. 16. Structure of the Por/C_{60}-Fc_2 rotaxane ensemble **35** [46].

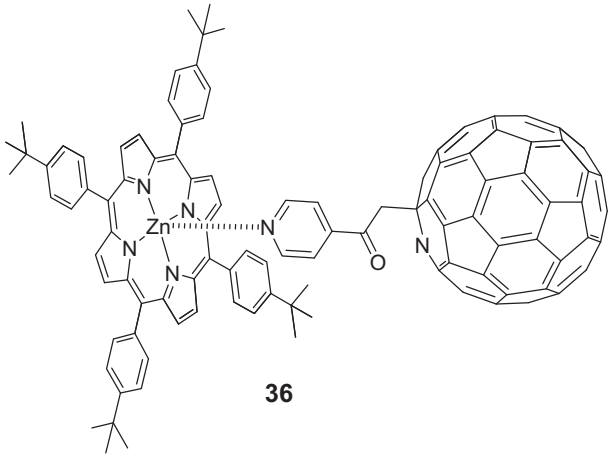

Fig. 17. Molecular structure of Zn(II)Por/$C_{59}N$ heterofullerene dyad **36** [50].

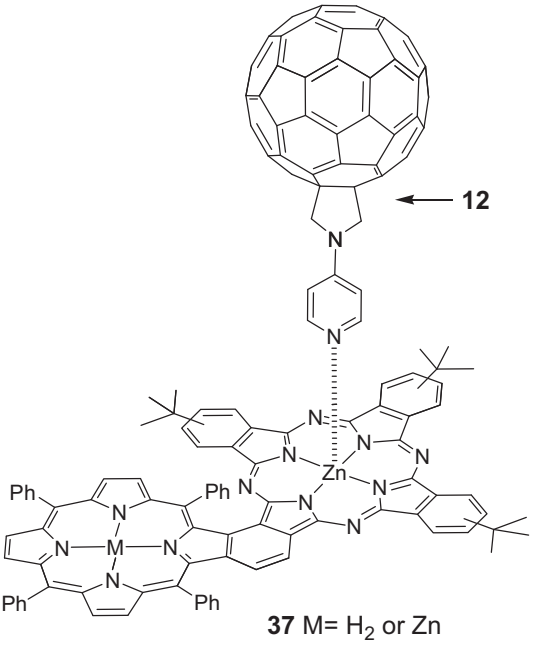

Fig. 18. Molecular structures of supramolecular Por-Zn(II)Pc/C_{60} triads **37** [51].

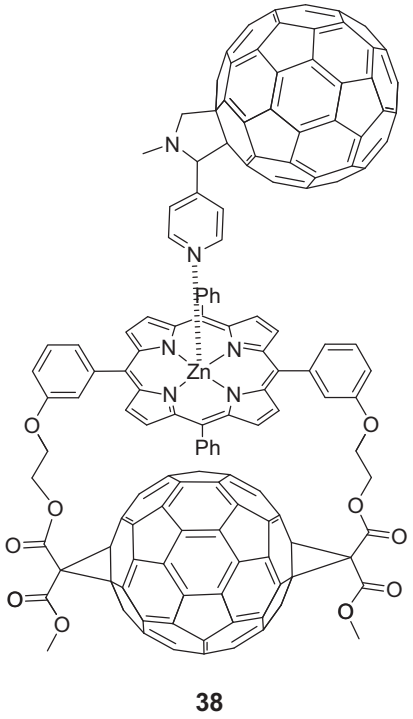

Fig. 19. Molecular structure of the Zn(II)Por-C_{60}/C_{60} triad **38** [53].

higher than those obtained for Zn(II)Por/C_{60} **24**. Depending on the solvent, either photoinduced singlet–singlet energy transfer or electron transfer was observed, the latter process taking place in *o*-DCB, leading to the corresponding charge-separated state Zn(II)Por$^{\bullet+}$/$C_{59}N^{\bullet-}$.

Covalently-fused, Pc–Por conjugates (**37**) have been prepared and complexed to fulleropyrrolidine **12** with the aim of preparing a D–A system able to harvest light over a broader spectrum range and to give rise to longer charge-separated lifetimes [51]. In triads **37**, a wide range of the solar spectrum was covered due to the complementary absorption of the Por and Pc components, whereas direct linkage of these macrocycles gave rise to strong mutual electronic coupling shifting the majority of the absorption features into the red region (Fig. 18). Photophysical measurements on Pc–Por/C_{60} systems **37**, having the fullerene derivative **12** axially coordinated to the Zn(II)Pc macrocycle, revealed that, upon photoexcitation, intramolecular energy transfer from the Por tetrapyrrole (either free-base or metallated) to the energetically lower-lying Zn(II)Pc macrocycle took place. This phenomenon is followed by an intramolecular CT from the excited Pc to C_{60}, leading to the Por-Zn(II)Pc$^{\bullet+}$/$C_{60}^{\bullet-}$ radical ion pair species formation. The deactivation of the transient radical ion pair to the ground state is then occurring without the formation of any charge shift reaction which would yield the Por$^{\bullet+}$-Zn(II)Pc/$C_{60}^{\bullet-}$ species.

Similarly to the case of Por-Zn(II)Pc/C_{60} triads **37**, a cascade of light induced energy and electron transfer processes was also observed for a series of Por-Zn(II)Pc conjugates, where the Pc has been directly linked to the β-pyrrolic position of a *meso*-TTP (free-base, Zn(II) or Pd(II)) and complexed via metal–ligand interaction to a *N*- or *C*-substituted, pyridine-bearing fulleropyrrolidine [52].

Another elegant approach toward the design of efficient D–A couples with optimized performance consists in the incorporation in these structures of a secondary electron donor or acceptor moiety. In this context, triad system **38** was prepared in which a fulleropyrrolidine ligand was axially coordinated to a π–π stacked Por–C_{60} conjugate (Fig. 19) [53]. Photophysical studies showed that, addition of variable concentrations of the C_{60} ligand failed to show any meaningful effect on the fluorescence quantum yield of ensemble **38**. Indeed, upon generating the Por singlet excited-state, deactivation of the latter occurs mainly via rapid electron transfer from the Zn(II)TPP entity to the π–π stacked fullerene, whereas the competing electron transfer process to the coordinated fullerene was too slow. However, upon generation of the fullerene singlet excited-state, a two-step intra- and intermolecular relaxation process has been detected, resulting in the formation of the Zn(II)TPP$^{\bullet+}$ and $C_{60}^{\bullet-}$ radical pair species which present a larger lifetime compared to the uncomplexed Por–C_{60} dyad.

A similar, mixed covalent-coordinate bonding approach has been applied for the preparation of ensemble **39** constituted by two Por electron-donor moieties and one C_{60} electron acceptor (Fig. 20) [54]. Supramolecular triad **39** is composed of a covalently-linked H_2Por-C_{60} dyad which is substituted on its fulleropyrrolidine part with a pyridine unit able to complex a Zn(II)TTP macrocycle. Study of the electrochemical behavior of the uncomplexed, covalent Por–C_{60} dyad in *o*-DCB revealed an efficient electron

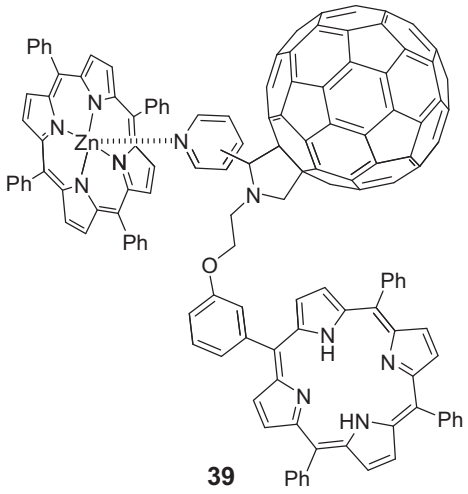

Fig. 20. Molecular structure of H_2Por-C_{60}/Zn(II)TTP supramolecular triad **39** [54].

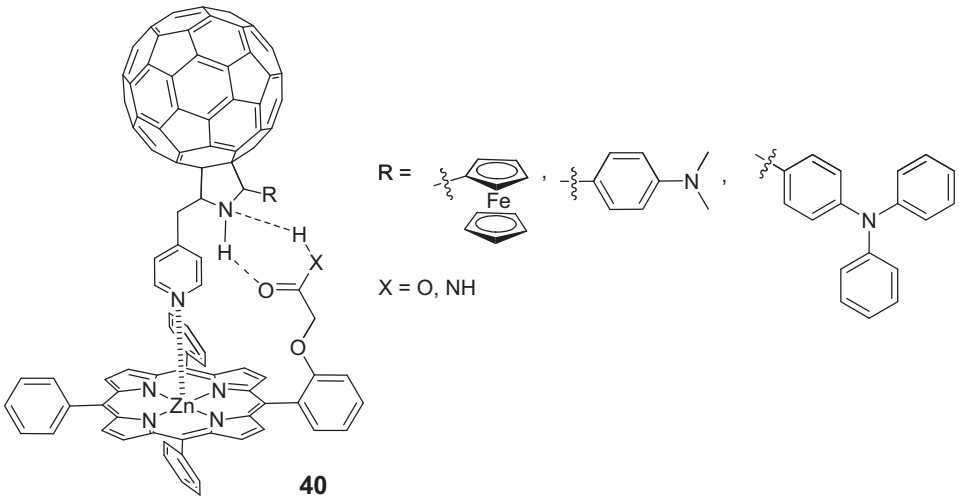

Fig. 21. Molecular structures of the supramolecular Zn(II)Por/C_{60} systems **40** assembled by a 'two-point' binding motif [56].

transfer from the singlet excited H_2Por moiety to the covalently-attached fullerene. Steady-state and time-resolved fluorescence measurements carried out on triad **39** in *o*-DCB showed a significant quenching of the Zn(II)TPP emission upon addition of the pyridine-substituted H_2Por-C_{60} dyad. Interestingly, the presence of a second donor in a triad **39** accelerates the CS process in *o*-DCB with respect to the uncomplexed H_2Por-C_{60} dyad.

A triad system structurally similar to **39**, in which a pyridine-substituted C_{60} bearing a H_2Por macrocycle coordinates to a Fe(II)TTP unit has also been reported [55]. Time-resolved emission and nanosecond transient absorption techniques carried out on this supramolecular triad put into evidence the occurrence of an electron transfer process, which, as in the case of **39**, was influenced by the presence of a coordinated, electron-donor Fe(III)PorCl macrocycle. The lifetime of the resulting charge-separated species was of the order of 20 μs as obtained by monitoring the decay of the $H_2Por^{\bullet+}$ species at 620 nm, although a partial overlapping with the long-living triplet states of the Por was observed at this wavelength.

Supramolecular triads (**40**) composed of C_{60} as primary electron acceptor, Zn(II)Por as primary electron donor, and either Fc, *N*,*N*-dimethylaminophenyl (DMA), or *N*,*N*-diphenylaminophenyl (DPA) as a second electron-donor moiety were constructed via a 'two-point' binding motif involving metal–ligand axial coordination and hydrogen bonding formation (Fig. 21) [56]. Considering that the oxidation potentials of the second electron-donor moiety follows the trend: Fc > DMA > DPA, free-energy calculations suggested the possibility of the occurrence of sequential hole transfer in these supramolecular triads. Efficient electron transfer from the excited singlet state of Zn(II)Por to the fullerene entity was observed for all the triads in *o*-DCB. Longer charge-separated states were observed in the case of a Zn(II)Por bearing a carboxylic acid compared to a similar system substituted with an amide group.

A supramolecular triad **41** has been prepared in which a light-harvesting Bodipy unit is able to transfer its excitation energy (λ_{exc} = 388 or 502 nm) to a covalently-linked energy acceptor Por unit (Fig. 22) [57]. An efficient electron transfer process from the photoexcited Por macrocycle to the Im-appended fullerene acceptor is then taking place, as demonstrated by steady-state and time-resolved emission as well as transient absorption measurements, in a system which mimics some of the key events of natural photosynthesis.

A multiantenna system similar to **41** consisting of four Bodipy units covalently-linked to a central Zn(II)Por unit complexed to an Im-substituted fullerene has also been prepared and investigated [58]. Photophysical studies on this multicomponent system revealed the occurrence of an efficient, and ultrafast (28–48 ps), singlet–singlet energy transfer from the peripheral Bodipy units to the central Zn(II)Por macrocycle. By increasing the number of Bodipy antenna units, a decrease in the energy-transfer lifetime has been observed.

A supramolecular system **42** constituted by a Zn(II)Pc covalently-connected to a Bodipy unit and axially coordinated to pyridine-substituted C_{60} **12** has also been reported (Fig. 23) [59]. The advantage of such system stems from the complementary absorption of the UV/vis part of the solar spectrum of the Pc (λ_{max} = 680 nm) and Bodipy (λ_{max} = 525 nm). Upon photoexcitation of **42** at 480 nm, an intramolecular transduction of singlet excited-state energy occurs from the light-absorbing and energy-donating

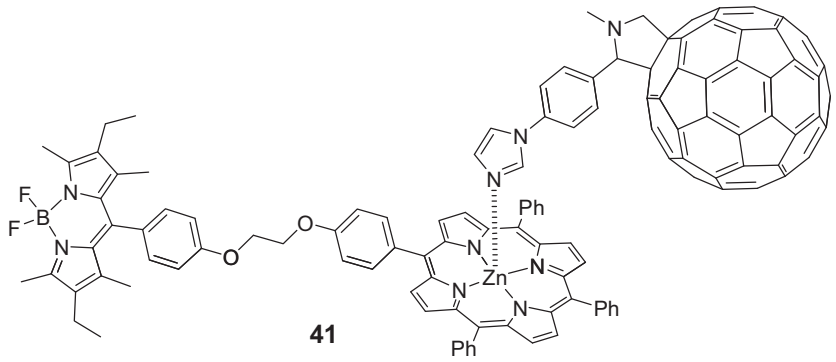

Fig. 22. Structure of Bodipy-Zn(II)Por/C_{60} triad **41** [57].

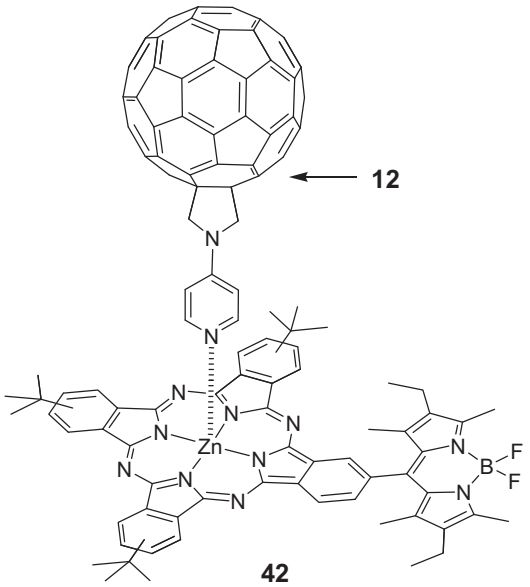

Fig. 23. Molecular structure of the Bodipy-Zn(II)Pc/C_{60} supramolecular triad **42** [59].

Bodipy to the energy-accepting Zn(II)Pc which then give rise to an electron transfer process towards the pyridine-substituted C_{60} ligand. Such cascade of processes finally generated a Bodipy-Zn(II)$Pc^{\bullet+}$/$C_{60}^{\bullet-}$ charge-separated species with a lifetime of 39.9 ns.

A supramolecular, tetracomponent system **43** having an Im-appended C_{60} axially coordinated to a SubPc-TPA-Zn(II)Por triad has also been prepared and studied by steady-state and transient absorption spectroscopy (Fig. 24) [60]. The rationale behind the preparation of such complex structure resides in the possibility to efficiently harvest solar energy due to the increased absorption cross section provided by the combined action of the SubPc and the Por macrocycles. In such a system, the donor ability of the Zn(II)Por unit would be increased by the covalent attachment of an electron reach TPA entity to its *meso* position, whereas an electron deficient SubPc entity, with its high energy singlet state, would act as an energy transferring antenna unit towards the Zn(II)Por macrocycle. Electrochemical measurements on **43** revealed that the energy level of the radical ion pair state SubPc-TPA-Zn(II)$Por^{\bullet+}$/$C_{60}^{\bullet-}$ is located lower than that of the singlet and triplet states of the Zn(II)Por and the fullerene entities. Interestingly, a slow CR ($1.6 \times 10^5\ s^{-1}$) and a long lifetime of the charge-separated state (6.6 μs) were obtained in toluene by nanosecond transient measurements.

Recently, several D–A supramolecular systems constituted of multiple antenna centers have been prepared. Thus, a synthetic heptad **44** (Fig. 25) featuring a central hexaphenylbenzene unit substituted with two bis(phenylethynyl)anthracene moieties that absorb light in the 400–500 nm range, two Bodipy entities with absorption in the 450–550 and 330–430 nm range and two Zn(II)Por macrocycles has been prepared [61]. Compound **44** also comprises a C_{60} sphere substituted with two pyridine ligands which coordinate to the two Por macrocycles via metal–ligand axial coordination. It was demonstrated that in such system, which harvests light from the ultraviolet throughout the visible region up to 650 nm, singlet excitation energy is efficiently funneled from all four antenna units to the Por moieties. This energy-transfer process is then followed by electron donation from the excited Pors to C_{60} to generate a charge-separated species which has a lifetime of 230 ps and an overall quantum yield close to unity.

Complex systems comprising several electron donor and acceptor units held together via multiple supramolecular interactions have also been prepared. In this context, a chiral, helical system **45** consisting in a Por-appended foldamer hydrogen bonded to six chiral, histidine-substituted C_{60} units has been reported (Fig. 26) [62]. The formation of **45** results from the cooperation of two discrete, noncovalent interactions: Zn(II)Por/Im metal–ligand coordination and Zn(II)Por/C_{60} π–π stacking interactions. At low concentration of foldamer and fullerene, a 1:6 stoichiometry was observed for **45** as revealed by UV/vis Job plot analysis. Fluorescence studies on **45** and reference compounds constituted of shorter, oligomeric units revealed that (i) the emission of the Zn(II)Por units are significantly quenched by the presence of the fullerene guests, and that (ii) the quenching increases with the elongation of the oligomers, this latter result supporting the existence of a cooperative effect for the complexation of the C_{60} guests by the Por oligomers. The apparent K_a of complex **45** determined by UV/vis and fluorescence titration experiments was of the order of $10^4\ M^{-1}$.

A similar, multicomponent system (**46**) consisting in a central benzene unit surrounded by six Zn(II)Por macrocycle, each of them coordinating to a pyridine-substituted fulleropyrrolidine moiety has been reported (Fig. 27) [63]. The aggregation ability of this system has been demonstrated by UV/vis studies whereas fluorescence experiments indicate that the emission of the Por receptors is strongly quenched by the coordinated fullerene units. Fluorescence titration experiments revealed a positive cooperative effect for the assembly of the C_{60}-pyridine derivatives with the polytopic Por receptor probably as a result of intramolecular C_{60}–C_{60} interactions between the numerous C_{60} guests assembled onto the multi-Zn(II)Por platform.

More recently, an artificial, photosynthetic model system constituted by a dendritic structure bearing 16 light-harvesting, Zn(II)Por moieties each of them axially coordinated to a fulleropyrrolidine C_{60} ligand was also reported [64]. In such supramolecular

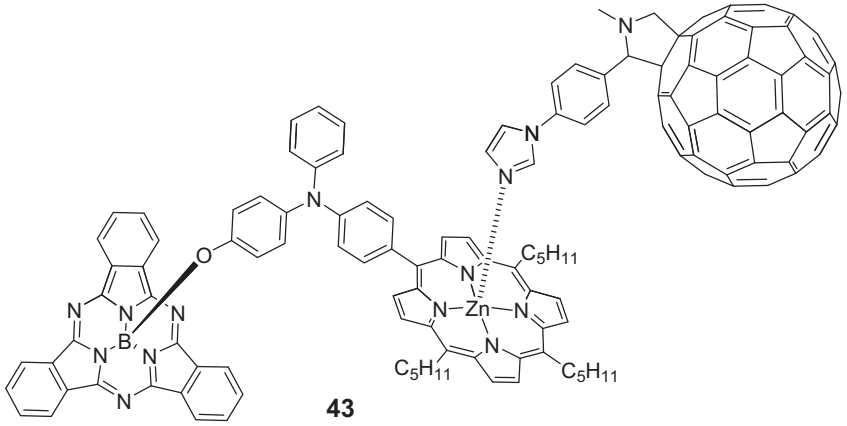

Fig. 24. Molecular structure of the SubPc-TPA-Zn(II)Por/C_{60} supramolecular tetrad **43** [60].

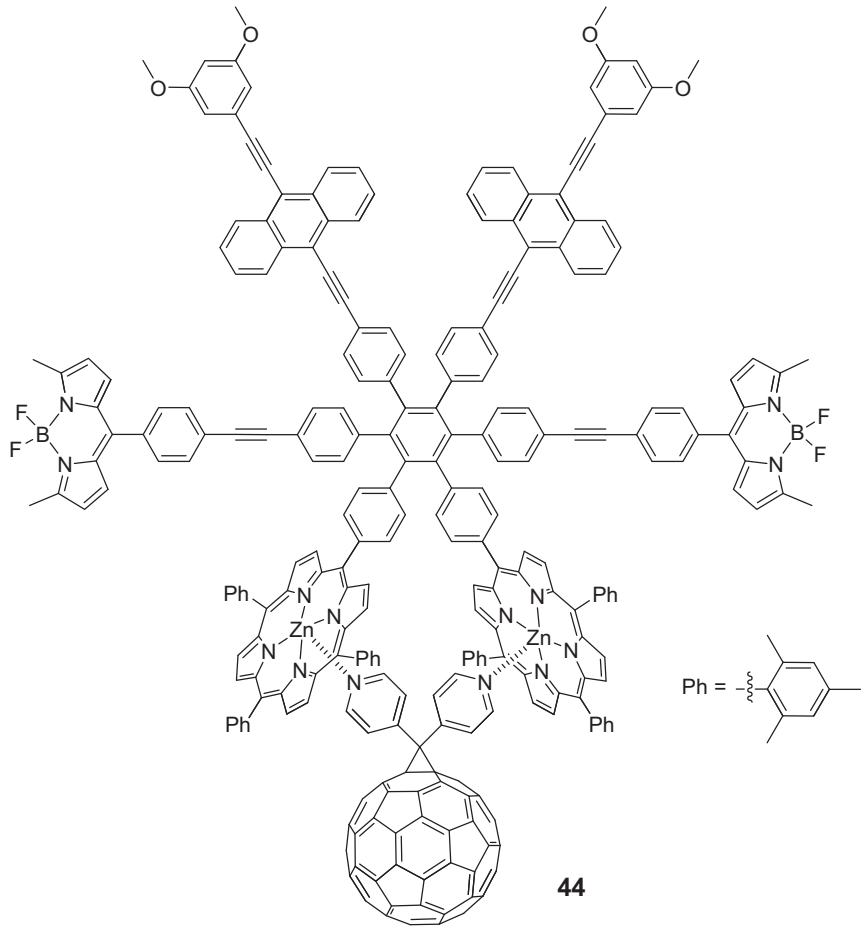

Fig. 25. Molecular structure of heptamer **44** [61].

complex, photoexcitation of the Por units leads to an efficient energy migration between the chromophores followed by a CS process. The lifetime of the charge-separated state of the supramolecular complex in benzonitrile and at room temperature was 0.25 ms, which is one of the longest lifetimes ever reported for a supramolecular complex based on Por and fullerene.

A larger stabilization of the charge-separated state lifetime has been observed for a D–A supramolecular ensemble constituted of multiple, light-harvesting Zn(II)Por and C_{60} units, and held together by a combination of coordination bond and π–π interactions [65]. The system consists of an oligopeptide bearing various Zn(II)Por pendant units (i.e., 2, 4 or 8) which are axially coordinated to fulleropyrrolidine units bearing a pyridine or an Im coordinating ligand. Photophysical studies on these supramolecular complexes revealed that, upon photostimulation, energy migration occurs between the Por units followed by a CS process. For such oligopeptide ensembles, an increase in the charge-separated lifetimes was observed with increasing number of the Por macrocycles, obtaining, in the case of the Por octamer complexed to the Im-substituted fullerene, a lifetime for the charge-separated state of 0.84 ms in benzonitrile and at room temperature.

The photovoltaic properties of some Por- or Pc/C_{60} supramolecular systems have also been investigated. Thus, for example, spin-coating a film of a fulleropyrrolidine bearing three pyridyl groups on a vacuum evaporated layer of Zn(II)Pc resulted in a solar cell showing better performance than a similar cell obtained by spin-coating PCBM over a Zn(II)Pc evaporated layer [66]. This result was rationalized invoking the formation of a supramolecular complex between the trispyridine-substituted C_{60} and the Zn(II)Pc at the bilayer interface, which enhances the CT between the donor and the acceptor components and, indeed, increases the photovoltaic performance of the device.

A similar concept has been used in order to prepare a high-performance, blend-type, parallel tandem solar cell having an active layer formed by blending three Pc derivatives presenting different optical band gaps in order to capture a larger fraction of the solar spectrum and a pyridine-substituted fullerene which can coordinate to the Zn(II)Pc axial position, thus facilitating an efficient exciton dissociation and electron transport to the electron-collecting contact [67].

The photoelectrochemical behavior of an Im-substituted C_{60} self-assembled via metal–ligand axial coordination to an electrochemically-polymerized Zn(II)Por film was also investigated [68]. A Zn(II)Por, bearing four electropolymerizable TPA substituents was first electropolymerized on the electrode surface to form a film. Absorption and emission studies carried out on the film revealed the characteristic absorption and emission features of the Por macrocycle indicating no significant changes of the π-electron system of the Por moiety in the polymer. Next, successful immobilization of an Im-substituted C_{60} fullerene to the Por units in the polymer film was achieved via metal–ligand axial coordination as revealed by cyclic voltammetry studies. Photoelectrochemical studies on such Por polymer/C_{60} ensemble showed a cathodic photocurrent generation, a result not common for most of the dye-sensitized photoelectrochemical cells. Moreover, coordination of the Im-substituted fullerene to the Zn(II)Por film improved the photocurrent and photovoltage generation of the photoelectrochemical cell, showing an IPCE of nearly 2% at the Soret region of maximum absorption.

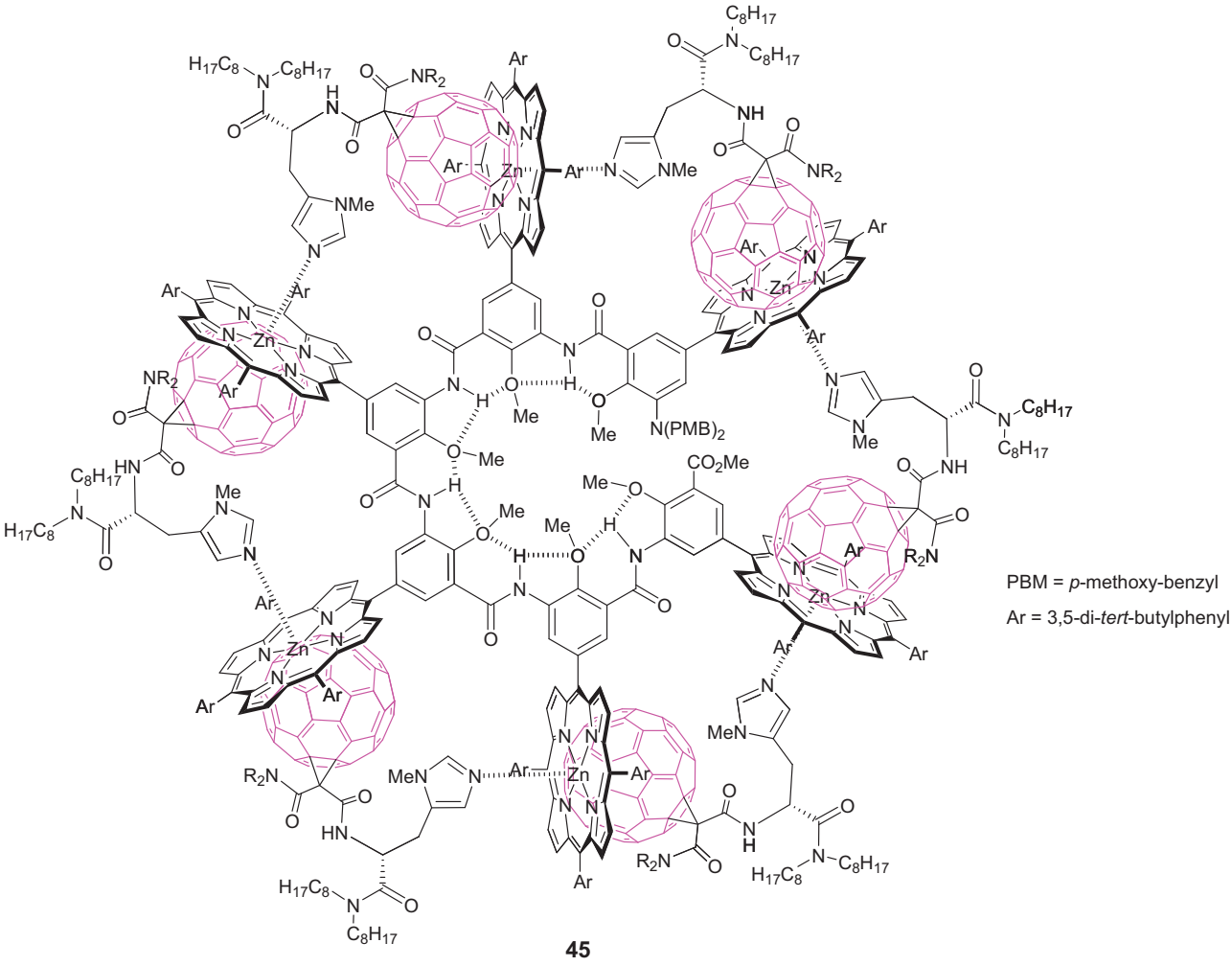

Fig. 26. Molecular structure of helical system **45** assembled through a combination of Por/Im metal–ligand coordination and Zn(II)Por/C_{60} π–π stacking interactions [62].

Recently, a supramolecular, D–A system based on Por and C_{60} units self-assembled on a flat, SnO_2 electrode has also been prepared and used as a photoelectrochemical device (Fig. 28) [69]. In such system, a Pd-mediated stepwise self-assembly of Zn(II)Por donors ensures the vertical growth of the Por rods on the SnO_2 electrode. On the other hand, pyridine-substituted fullerene acceptors are infiltrated into the Por linear arrays self-assembling on the macrocycles through metal–ligand axial coordination and π–π interactions. For such system, the relationship between the film structure in the device and its photoelectrochemical properties has been elucidated as a function of the number of donor layers, obtaining a maximum IPCE value of 21%, which is among the highest reported value for vertical arrangements of bicontinuous D–A arrays on electrodes.

3. Porphyrin- and phthalocyanine–C_{60} covalent systems presenting long-range order

Supramolecular interactions have also been used in order to assemble covalent Por- or Pc–C_{60} fullerene [70] systems over large length scales. The possibility to self-assemble these covalent, D–A conjugates is highly desirable since such organization often leads to an improvement of some of the chemical and physical properties presented by these self-assembled systems with respect to their molecularly-dispersed counterparts, an aspect particularly important especially for molecular photovoltaics and field effect transistor applications, where the order of both the fullerene and the donor components in the solid state is a key issue for achieving high carrier mobilities.

Within the "toolbox" of supramolecular interactions that have been used to self-assemble covalent Pc-fullerene systems, the combination of π–π stacking and liquid-crystalline interactions is particularly attractive because, in appropriately substituted Pc macrocycles, it allows generation of highly ordered, stacked, columnar supramolecular ensembles. In this context, few reports have appeared on the preparation of fully mesogenic Pc–C_{60} dyads [71,73].

In a report by Geerts et al., a series of mesogenic Pc–C_{60} dyads (**47a–d**) was prepared by an esterification reaction between unsymmetrically substituted Pcs bearing a terminal alcohol group and a fullerene derivative bearing a terminal acid moiety (Fig. 29) [71]. The thermotropic properties of these dyads were studied by POM and DSC revealing the formation of liquid-crystalline mesophases only in the case of Pc–C_{60} ensembles **47c**,**d**, suggesting that a long spacer is needed in order to allow the bulky C_{60} moiety to be accommodated in the columnar mesophase formed by the stacked Pc macrocycles.

Similarly, a mesogenic Pc–C_{60} dyad (**48**) has been reported by Torres and co-workers, which consisted of a hexadodecyl-substituted Zn(II)Pc covalently-connected through a flexible spacer to a C_{60} fullerene via a Bingel-Hirsch cyclopropanation reaction (Fig. 29) [72]. Also in this case, POM and DSC studies on this dyad revealed liquid-crystalline behavior of this ensemble between 80

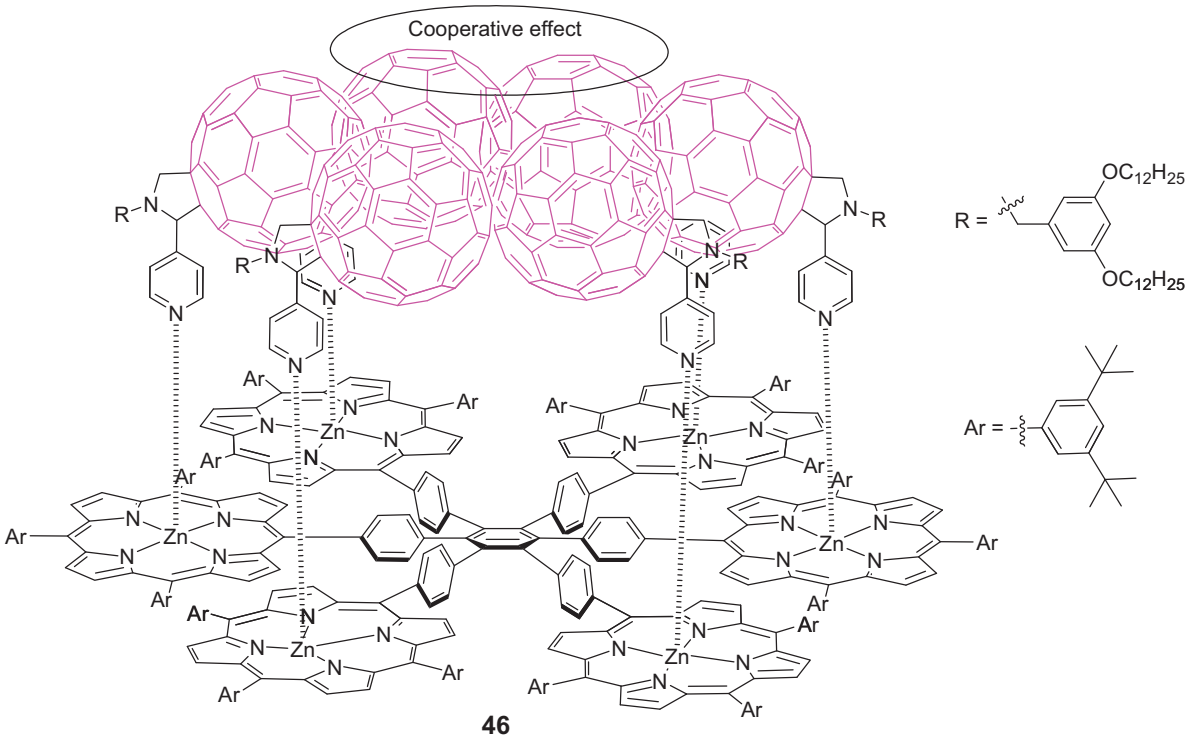

Fig. 27. Molecular structure of a hexameric Por derivative complexing six, pyridine-substituted C_{60} units leading to supramolecular complex **46** [63].

and 180 °C. Complementary XRD studies showed that Pc–C_{60} dyad **48** adopts a rectangular symmetry within the columnar mesophase (i.e., Col_r), each rectangular unit having a column at its center and four others at its corners.

More recently, a mesogenic, covalently-linked Zn(II)Pc–C_{60} dyad (**49**) able to self-assemble giving rise to the formation of segregated, liquid-crystalline columns was reported (Fig. 29) [73]. The D–A heterojunction structure formed by this Pc–C_{60} conjugate exhibits highly efficient, short-range and long-range charge-transport properties. Interestingly, when the liquid-crystalline material was heated, an increase of the total charge mobility of more than five times was observed with respect to the unheated samples. This phenomenon could be due to a better alignment of the Zn(II)Pc–C_{60} columns within the mesophase upon heating which may facilitate the charge transport between the Zn(II)Pc–C_{60} columns, thus leading to an improvement of the macroscopic charge mobilities.

In 2008, the first report on an indirect and easy way to incorporate a series of covalent Pc–C_{60} dyads into a liquid–crystalline architecture has appeared [74]. The strategy consisted of blending

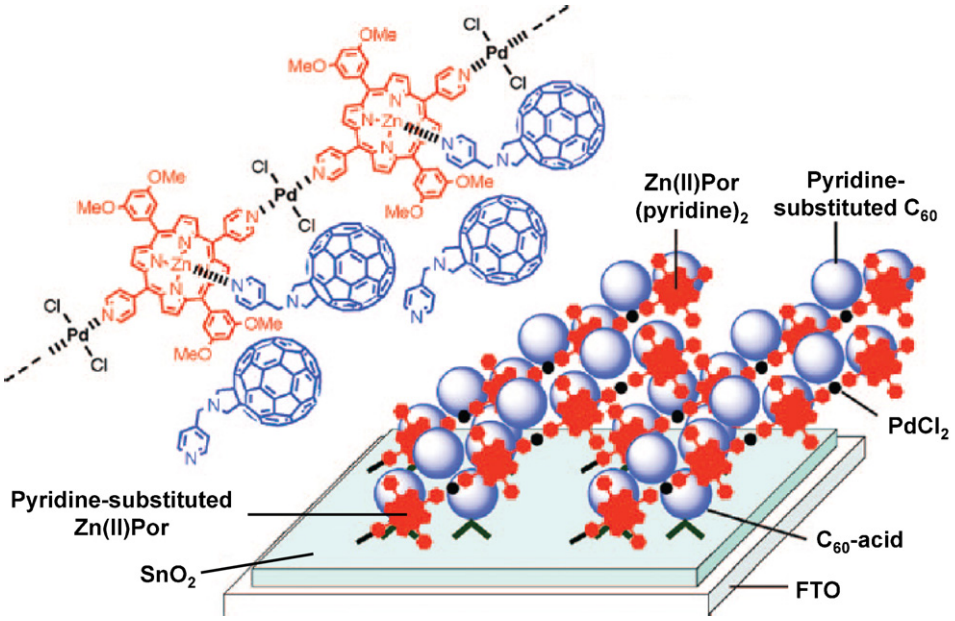

Fig. 28. Schematic representation of the Por/C_{60} arrays on a SnO_2 electrode.

Reprinted with permission from Ref. [69].

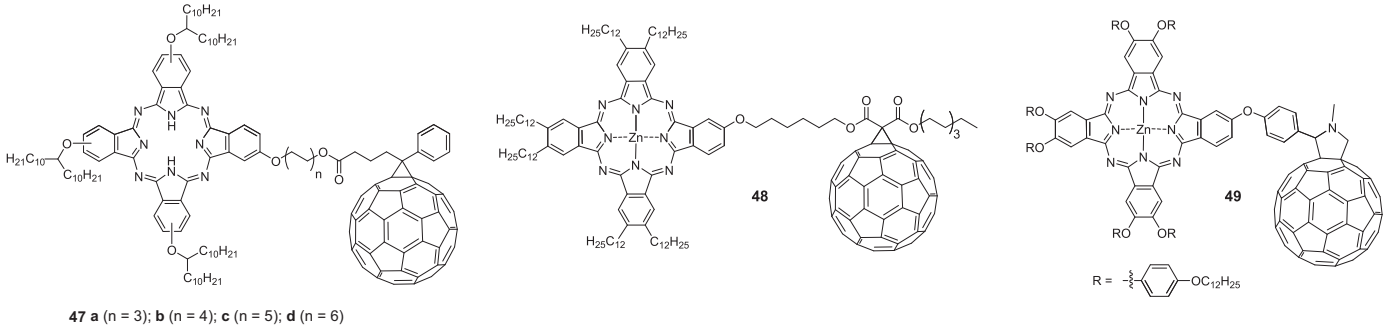

Fig. 29. Molecular structures of mesogenic Pc–C_{60} dyads **47** [71], **48** [72] and **49** [73].

a nonmesogenic Pc–C_{60} dyad with a mesogenic, symmetrically substituted Zn(II)Pc. XRD studies of equimolecular mixtures of these two Pcs resulted in the formation of hexagonal columnar mesophases at ~60–70 °C in which the liquid–crystal columns were composed of an alternating stack of mesogenic Pc and Pc–C_{60} dyad. The use of blends, in which a mesogen is able to induce mesomorphism on a nonmesogenic Pc-based functional material, represents an interesting strategy for the incorporation of photoactive, D–A Pc–C_{60} systems in a liquid–crystalline architecture.

The formation of long-range ordered, Pc–C_{60} nanoensembles formed through a combination of π–π stacking and hydrophilic–hydrophobic interactions has also been reported using an amphiphilic Pc–C_{60} dyad (**50**, Fig. 30a) [75]. UV/vis and light-scattering studies showed that such a D–A conjugate strongly aggregates when dispersed in water, giving rise to the formation of uniform, micrometer-long nanorods as revealed by TEM experiments (Fig. 30b). Steady-state and transient absorption studies demonstrated that the self-organization ability of the amphiphilic ensemble **50** in water also had a profound influence on the photophysical properties of these 1-D nano-objects. Particularly, transient absorption measurements on these nanotubules of **50** revealed the formation of a long-lived photoinduced CT product. For such a system, an impressive stabilization of more than six orders of magnitude was observed for the charge-separated lifetime of self-assembled dyad **50** (i.e., 1.4 ms) with respect to a structurally related Pc–C_{60} dyad analogous to **50**, which lacks the terminal ammonium unit and which is not able to form nanotubules (i.e., ~3 ns).

Interestingly, similar nanotubular objects with dimensions typically reaching 30 nm in diameter and 500 nm in length were obtained by dispersing in water an amphiphilic Por–C_{60} dyad structurally related to **50** [76]. In such system, Por/Por, Por/C_{60}, and C_{60}/C_{60} interactions are the driving forces of the self-assembly of this covalent conjugate.

Supramolecular interactions have also been used to promote the organization of a structurally rigid, covalently-linked Pc–C_{60} conjugate (**51**, Fig. 31a) on solid surfaces [77]. Dyad **51** is able, when drop-casted from toluene solutions, to self-organize on highly ordered pyrolytic graphite (HOPG) and graphite-like (i.e., graphite oxide) surfaces giving rise to the formation of micrometer-long fibers and films as revealed by AFM experiments (Fig. 31b). Conductive AFM measurements were carried out on such supramolecular fibers and films in order to address the electrical properties of these nanostructures obtaining electrical conductivity values as high as 30 μA for bias voltages ranging from 0.30 to 0.55 V. Control experiments revealed that the high electrical conductivity values observed for this solid-supported, self-assembled Pc–C_{60} conjugate were strongly related to the supramolecular order of the dyad within the nanostructures.

The same Pc–C_{60} dyad **51** was also able to self-organize by means of noncovalent interactions on the outer wall of SWCNTs grown by chemical vapor deposition on a silica surface [78]. In such a study, the strong affinity of dyad **51** for graphitic surfaces (vide supra) coupled to the poor affinity of this conjugate for hydrophilic surfaces such as silica has been exploited in order to promote the long-range organization of **51** on the curved, 1-D, graphite-like surface of the SWCNTs.

Self-assembled monolayers (SAMs) of covalently-linked MPor-C_{60} (i.e., M = H_2 or Zn(II)) dyads have also been prepared on ITO and gold surfaces and the photovoltaic properties of these D–A conjugates investigated [79,80]. These studies showed that a stable cathodic photocurrent appears immediately upon light irradiation (λ_{exc} = 430 nm) of the H_2Por-C_{60} SAMs on ITO electrode, whereas the photocurrent fell down instantly when the irradiation was cut

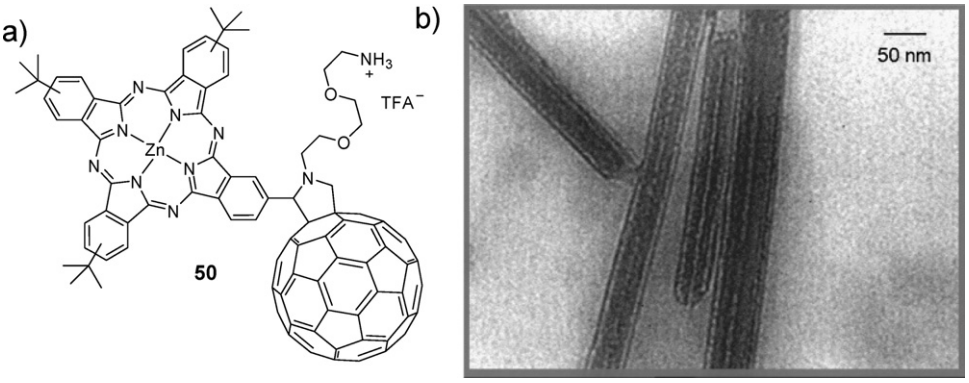

Fig. 30. a) Molecular structure of Pc–C_{60} dyad **50**. b) TEM image of the nanotubules formed by dyad **50** in water. The image in b) is reprinted with permission from Ref. [75].

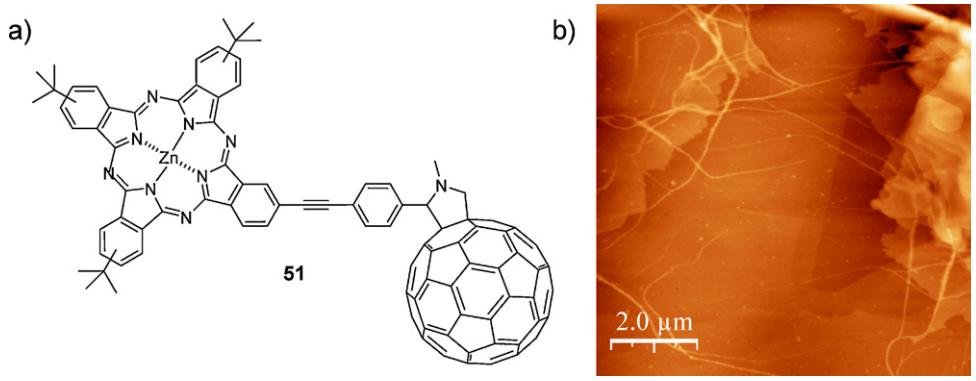

Fig. 31. a) Molecular structure of Pc–C_{60} conjugate **51**. b) AFM topographic image of dyad **51** drop-casted on HOPG. The image in b) is reprinted with permission from Ref. [77].

off. Control experiments showed that the remarkable enhancement of the photocurrent generation in the Por–C_{60} systems was due (i) to the incorporation of C_{60} as an electron acceptor into the Por SAMs on ITO and (ii) to the well-packed structures of the H_2Por-C_{60} molecules in the SAMs with the dyads covering the ITO surface uniformly as demonstrated by AFM measurements.

4. Porphyrin- and phthalocyanine/carbon nanotube supramolecular systems

Similarly to fullerenes, carbon nanotubes [9] can also act as electron acceptor materials when coupled with appropriate electron-donor dyes. There are two general approaches for the functionalization of carbon nanotubes: (i) through the use of noncovalent, π–π interactions between appropriately functionalized molecules and the nanotube wall, or (ii) by covalent attachment of organic molecules to the carbon nanotube open edges or side walls. While the covalent approach leads to more thermodynamically stable structures, the noncovalent functionalization presents the advantage that the electronic structure of the nanotube remains almost unaffected.

In the following section, we will present some representative examples in which Pors or Pcs have been connected to carbon nanotubes using π–π interactions (Section 4.1) or via axial coordination of these macrocycles to carbon nanotubes covalently-functionalized with nitrogenated ligands (Section 4.2), giving rise, in both cases, to the formation of supramolecular, Por- and Pc/carbon nanotube ensembles.

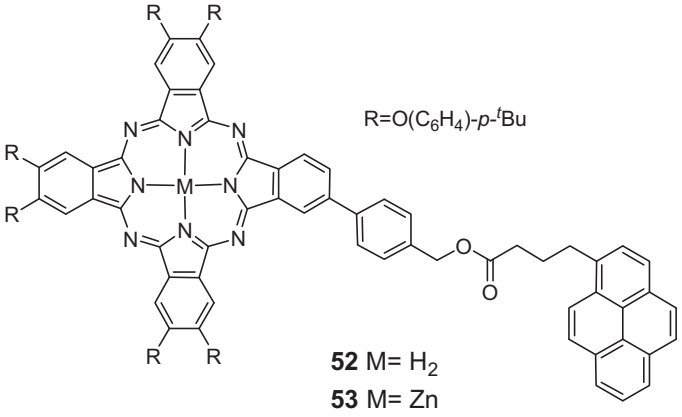

Fig. 32. Molecular structures of Py-substituted Pcs **52** and **53** [82].

4.1. Porphyrin- and phthalocyanine/carbon nanotube supramolecular systems assembled through π–π interactions

The noncovalent functionalization of pristine carbon nanotubes with appropriately derivatized, electron-donor chromophores represents an interesting strategy for the preparation of D–A, carbon nanotube-based ensembles, since it fully preserves the excellent electronic properties of these tubular nanoobjects. Such "supramolecular" approach, leading to the immobilization of the dyes onto the carbon nanotubes sidewall, is highly desirable especially for application of these carbon nanotube-based materials in the field of optoelectronics and photovoltaics.

Until now, a variety of supramolecular assemblies based on Pcs or Pors and SWCNTs have been reported by means of Py/SWCNT supramolecular interaction, taking advantage of the strong π–π interactions of Py to the SWCNT sidewalls [81]. In this context, Py-substituted, free-base (**52**) and zinc(II) (**53**) Pcs have been prepared and their interactions with SWCNTs probed (Fig. 32) [82].

The formation of stable, **52**/SWCNT and **53**/SWCNT supramolecular complexes has been demonstrated by means of various spectroscopic and microscopic techniques. UV/vis and steady-state fluorescence titration studies carried out on a suspension of SWCNTs in THF with H_2Pc-Py **52** (or Zn(II)Pc-Py **53**) solutions revealed a significant broadening and red-shift of the Pcs Q-band absorption, as well as an important quenching of the Pcs fluorescence. The formation of such Pc-Py/SWCNT complexes was also inferred by the red-shift of the SWCNTs NIR absorption and the quenching and red-shift of the SWCNTs fluorescence, a phenomenon due to the occurrence of a CT dynamics between the Pc donor and the SWCNT acceptor moieties as demonstrated by transient absorption measurements. AFM measurements carried out on Pc-Py/SWCNT dispersions showed the presence of well-dispersed thin bundles of SWCNTs, thus suggesting the successful immobilization of the Pc-Py species onto SWCNTs. The absence of any structural damage of the nanotube upon the Pc-Py functionalization was demonstrated by Raman measurements carried out on liquid and solid samples of Pc-Py/SWCNT which did not show any change in the G- or D-bands of the SWCNTs with respect to the pristine SWCNT sample. In order to test the solar energy conversion potential of such Pc/SWCNT ensembles, Pc-Py/SWCNT thin films have been prepared and their photovoltaic properties investigated. These studies revealed the formation of stable and reproducible photocurrents with monochromatic internal photoconversion efficiency values, for the H_2Pc-Py/SWCNT hybrid material **52**, as large as 23 and 15%, with and without an applied bias of +0.1 V, respectively.

A similar strategy has been used to "anchor" a single-molecule magnet (SMM) complex – a molecular species that displays slow dynamics of the magnetization at low temperatures and an

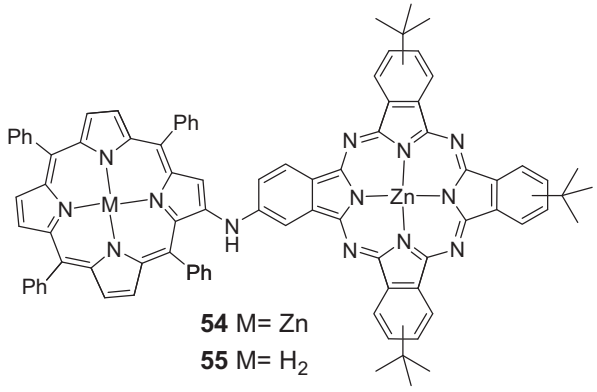

Fig. 33. Molecular structures of Pc–Por dyads **54** and **55** [84].

impressive array of quantum features – constituted by a heteroleptic bis(phthalocyaninato) terbium(III) complex bearing a Py unit to SWCNTs [83]. A combination of characterization techniques such as TEM, emission spectroscopy, coupled plasma atomic emission spectroscopy, and AFM were carried out on the SMM/SWCNT hybrid with a loading of the SMM complex within the supramolecular ensemble of one molecule every 7–8 nm of SWCNT length. Magnetization studies on such a SMM/SWCNT conjugate revealed that the SMM behavior of the heteroleptic complex is not only retained but also improved in the hybrid material.

More recently, a modification of the Pc-Py concept seen above for the preparation of Pc-Py/SWCNT ensembles has been presented, in which the Py moiety has been replaced by a Zn(II)TTP (**54**) or H_2Por (**55**) unit, linked through its β-pyrrolic position to a Zn(II)Pc (Fig. 33) [84]. A first insight on the occurrence of supramolecular interactions between the Pc–Por dyads and SWCNTs was inferred by UV/vis titration experiments in which a slight red-shift of both the Por Soret band and the Pc Q-band was observed upon the addition of a SWCNT suspension to solutions of **54** or **55**. Fluorescence studies carried out on Pc–Por dyads **54** or **55** alone revealed that, upon photostimulation of the Por unit at 410 nm, a rapid and effective energy-transfer process takes place from the Por to the Pc moiety (i.e., complete quenching of the TPP fluorescence and emission from the Pc unit). On the other hand, the same experiment carried out in the presence of a dispersion of SWCNTs resulted in a considerable quenching of the Pc emission. These observations suggest that Pc–Por dyads **54** or **55** interacts strongly with dispersed SWCNTs through the Zn(II)Pc moiety, while the interactions through the Por macrocycle seem to be intrinsically weak, thus implying a transduction of the singlet excited-state energy from the TPP to the Pc followed by a CT mechanism to the SWCNTs. This mechanism was finally confirmed by transient absorption studies, which revealed a rapid deactivation of the Pc singlet excited-state and the synchronous appearance of the spectroscopic "fingerprints" of the Pc radical cation and reduced SWCNT species.

A combination of Py/SWCNT π–π stacking and metal–ligand coordination interactions has also been used for the preparation of the sophisticated, three-component, supramolecular systems Zn(II)Nc/Im-Py/SWCNT **56** or Zn(II)Por/Im-Py/SWCNT **57** (Fig. 34) [85,86]. Key for the realization of such assemblies is the Im-substituted Py (Im-Py) compound which acts as a "bridging" unit for these supramolecular ensembles thanks to the phenylimidazole moiety which is able to strongly coordinate to the zinc center of the Nc or Por macrocycles while interacting with the SWCNT surface through the Py moiety.

Evidences for the formation of Zn(II)Nc/Im-Py/SWCNT or Zn(II)Por/Im-Py/SWCNT ensembles was supported by absorption and fluorescence titration studies. The absorption of Zn(II)Nc or Zn(II)Por upon addition of Im-Py/SWCNT resulted in spectral changes in which the intensity of the Zn(II)Nc Q-band or Zn(II)Por Soret band diminished, whereas a quenching and red-shift of the emission bands of the macrocycles was observed with respect to the uncomplexed Zn(II)Nc or Zn(II)Por systems. The Zn(II)Nc and Zn(II)Por compounds were also titrated against a Py/SWCNT ensemble in which the Py derivative did not have the Im moiety. In such experiments, the fluorescence quenching of the chromophores was less (i.e., 25%) than that of **56** or **57**. This result

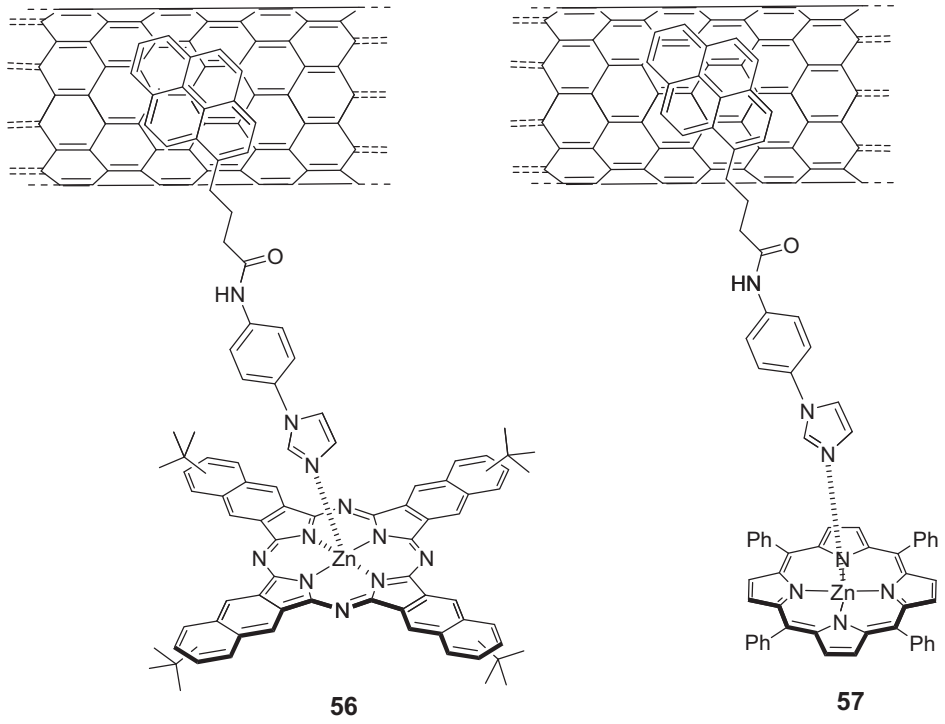

Fig. 34. Noncovalent assembly of SWCNT and Zn(II)Nc (**56**) or Zn(II)Por (**57**) using an Im-substituted Py bridging compound [85,86].

suggests that the axial coordination between the zinc metal of the macrocycles and the Im entity in the bridging Im-Py compound facilitates the nanohybrid formation. Nanosecond transient absorption spectra carried out on both macrocycle/Im-Py/SWCNT ensembles revealed that the photoexcitation of the Zn(II)Nc or Zn(II)Por moiety resulted in the one-electron oxidation of the donor unit and the simultaneous one-electron reduction of the SWCNT species, leading to the formation of the charge-separated species $Zn(II)Nc^{\bullet+}$/Im-Py/$SWCNT^{\bullet-}$ and $Zn(II)Por^{\bullet+}$/Im-Py/$SWCNT^{\bullet-}$. An additional proof for the occurrence of photoinduced CS for these ensembles was obtained by electron-pooling experiments in which the photogenerated cationic and anionic radical species $SWCNT^{\bullet-}$ and $macrocycle^{\bullet+}$ were used, in solution, to reduce an electron mediator and oxidize an electron-hole shifter compound, respectively.

In a similar "two-point" supramolecular approach, a functionalized Py "bridging" compound bearing a cationic, alkyl ammonium (i.e., Py-NH_3^+) or an anionic, carboxylate (i.e., Py-COO^-) moiety was loaded onto SWCNT to form positively charged Py-NH_3^+/SWCNT or negatively charged Py-COO^-/SWCNT hybrids. These ionic ensembles were then assembled via ion-pairing interaction with unsymmetrically substituted Zn(II) or H_2Pors bearing either anionic, sulfonatophenyl (in the case of Py-NH_3^+/SWCNT) or cationic, *N*-methylpyridyl groups (in the case of Py-COO^-/SWCNT), giving rise to the formation of stable D–A nanohybrids [87]. For such ensembles, the occurrence of a PET process from the singlet excited-state of the Por macrocycle to the carbon nanotube was confirmed by steady-state and time-resolved emission studies.

A combination of π–π and ammonium-crown ether interactions have also been used to assemble a Zn(II)Por/Py/SWCNT hybrid (**58**), constituted by a Por macrocycle peripherally substituted with four crown ether moieties and a Py "bridging" unit bearing an alkyl ammonium cation group (Fig. 35) [88]. The presence of four crown ether moieties on the Por macrocycle able to complex multiple SWCNT-immobilized, ammonium-substituted Py units led to the formation of extremely stable supramolecular Zn(II)Por/Py/SWCNT complexes.

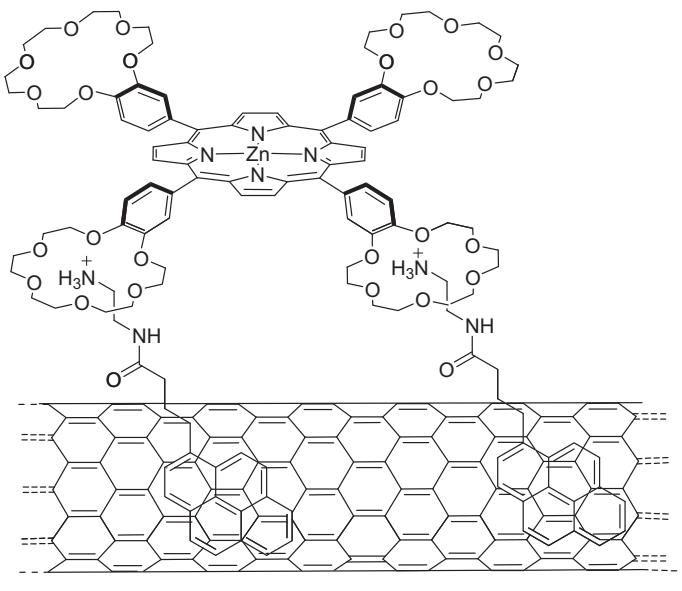

58

Fig. 35. Noncovalent assembly of SWCNT and Zn(II)TTP using an ammonium-substituted Py bridging compound (**58**) [88].

More recently, a Zn(II)Por macrocycle covalently-substituted with four peripheral Py unit (i.e., Zn(II)Por-Py_4) has been prepared and its interaction with (7,6)- and (6,5)-enriched, semiconducting SWCNTs investigated [89]. Transient absorption studies demonstrated that efficient CS takes place between the singlet excited-state of the Zn(II)Por and both the (7,6)- and (6,5)-enriched SWCNTs, as confirmed by the observation of the Zn(II)Por radical cation species. Interestingly, (7,6)-SWCNTs ensembles resulted to be slightly better in terms of charge stabilization compared to the (6,5)-SWCNTs ensembles. Photovoltaic devices were fabricated using the Zn(II)Por-Py_4/SWCNT hybrid. A maximum of 1% of IPCE was obtained at 420 nm for the (7,6)-SWCNT ensembles, a value three times larger than that of (6,5)-SWCNT.

D–A, Pc/SWCNT supramolecular hybrids based on a series of dendritic (i.e., first to third generations), electron-donor H_2Pcs have also been recently reported [90]. In such systems, the dendritic nature of the oligoethylene-functionalized Pcs as well as their π-extended aromatic surface allow effective interaction of the Pc core to the surface of the SWCNTs without the requirement of any Py anchoring group (Fig. 36). In the case of the third-generation-dendrimer, Pc/SWCNT ensemble, a particularly stable complex was obtained as demonstrated by a series of optical and microscopy techniques. Once again, transient absorption studies were carried out in order to shed light on the fate of the photogenerated products, suggesting the occurrence of a CT process between the Pc and SWCNT with the formation of the $Pc^{\bullet+}$ and $SWCNT^{\bullet-}$ species, with lifetime of about 250 ps. It is interesting to notice that the presence of dendritic oligoethylene glycol end groups allowed to disperse SWCNTs both in common organic solvents and in aqueous media.

Poly(*p*-phenylene vinylene) (PPV) oligomers containing Pc moieties covalently-linked, in the form of pending arms, to the oligomers backbone have also been prepared (**59** and **60**) and their interactions with SWCNTs studied (Fig. 37) [91]. Several techniques such as AFM, Raman, UV/vis, and NIR absorption demonstrated that oligomer **59** affords stable and finely dispersed SWCNTs' suspensions, whereas oligomers **60a**–**c** failed to disperse the carbon nanotubes. A possible explanation for these results resides in the different electronic character of these two classes of PPV oligomers. In the case of oligomer **59**, the presence of electron-withdrawing cyano substituents confer to the PPV oligomer a n-type character, thus favoring strong interactions with SWCNTs, which are p-type materials. On the contrary, PPV oligomers **60a**–**c** possess a p-type character that hampers the interactions with SWCNTs. Transient absorption measurements carried out on the **56**/SWCNT ensemble revealed the formation of a metastable charge-separated photoproduct.

However, supramolecular interactions have also demonstrated between SWCNTs and a long (i.e., 27 repeating units) PPV oligomer (**60d**) possessing a p-type character and having the Pc pendant units connected to the PPV backbone through a long spacer [92]. This

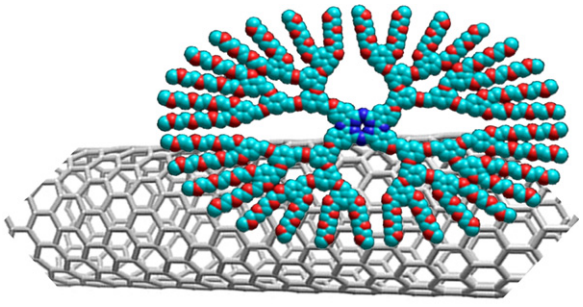

Fig. 36. Schematic representation of the noncovalent assembly of a third-generation, dendritic Zn(II)Pc onto a SWCNT [90].

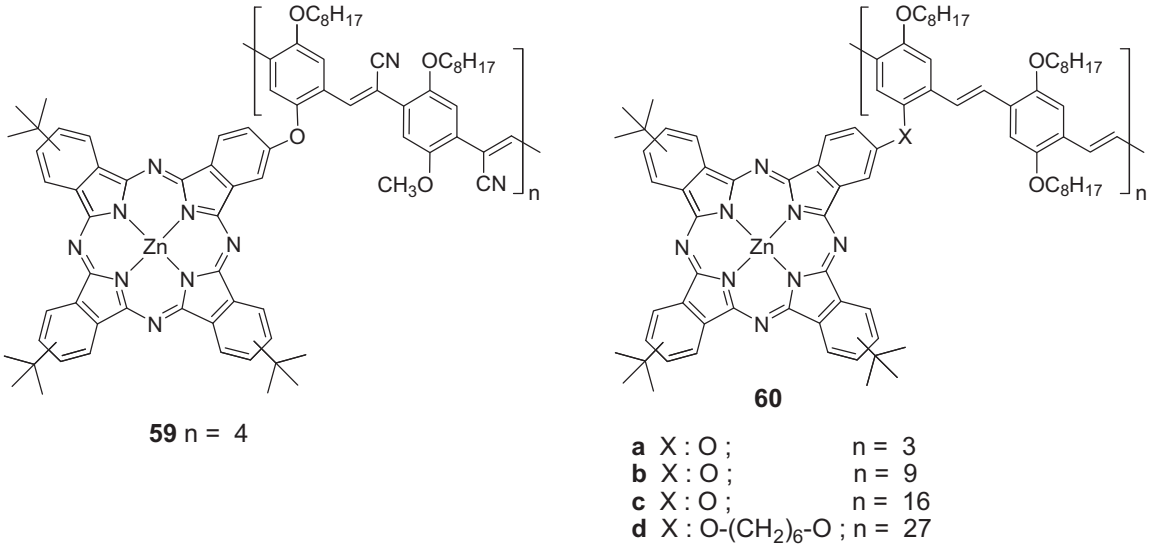

Fig. 37. Molecular structures of Pc-based PPV oligomers **59** and **60** [91].

study suggests that, beside the occurrence of n-type/p-type interactions between the SWCNTs and the Pc-based PPV oligomer, the structural flexibility of the oligomer also plays an important role.

Por polymers have also been used in order to disperse carbon nanotubes, as in the case of a conjugated Zn(II)Por polymer (**61**) which is able to strongly interact with the surface of SWCNTs, producing a soluble polymer-SWCNT ensemble (Fig. 38) [93]. Moreover, the interactions between the SWCNT and the Zn(II)Por units of the polymer result in the planarization and conjugation of the Por units, as inferred by a 127 nm bathochromic shift of the Por Q-band absorption from 796 to 923 nm. AFM studies indicated that the polymer can exfoliate the nanotube bundles and "stitch" multiple nanotubes together into a series of long, interconnected strands.

Supramolecular interactions between SWCNTs and a triply-fused Por system, have also been demonstrated [94]. Such Por/SWCNT complex was extremely stable in THF probably due to the extended, π-conjugated structure of the Por trimer and its enhanced electron-donating character. AFM studies carried out on such Por/SWCNT ensemble revealed that the Por trimer forms a uniform coating on the SWCNTs.

The production methods for SWCNTs generally yield mixtures of both metallic and semiconducting SWCNTs, which have different electrical properties, being important a complete separation of these two kinds of SWCNTs for different technological applications. An interesting example of the use of supramolecular interactions for the separation of metallic and semiconducting SWCNTs by using a H_2TTP derivative bearing four long alkoxy chains has been reported [95]. This separation method relies on the selective, non-covalent complexation of the derivatized Por toward the semiconducting SWCNTs, resulting in a significant enrichment of the semiconducting SWCNTs in the solubilized sample and predominantly metallic SWCNTs in the residual solid sample according to Raman, near-IR absorption, and bulk conductivity characterizations.

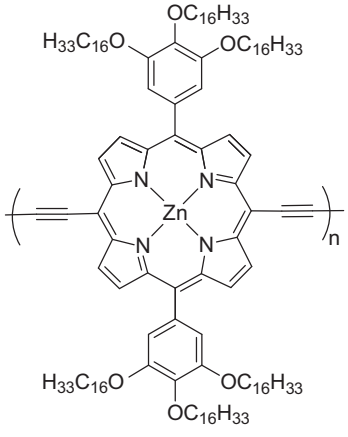

Fig. 38. Molecular structure of Zn(II)Por polymer **61** [93].

4.2. Porphyrin- and phthalocyanine/carbon nanotube supramolecular systems assembled via metal–ligand axial coordination

In contrast to the plethora of Por- and Pc/carbon nanotube supramolecular systems assembled via π–π interactions that have been reported, much scarcer are the examples of supramolecular ensembles constituted by carbon nanotubes covalently-functionalized with nitrogenated ligands which interact with Pors or Pcs via metal–ligand axial coordination.

In this context, a soluble, pyridine-functionalized SWCNT has been synthesized via 1,3-dipolar cycloaddition of a pyridine-substituted nitrile oxide compound on pentyl ester-functionalized SWCNTs. The resulting pyridine-substituted SWCNTs are able to complex Zn(II)TTP macrocycles in a way similar to that reported for pyridyl-functionalized C_{60} as revealed by optical and electrochemical studies (Fig. 39) [96]. However, in contrast to the behavior observed for the Zn(II)TTP/pyridine-substituted C_{60} complexes (vide supra), photochemical excitation of the Zn(II)TTP/SWCNT ensemble does not give rise to an electron transfer process with the generation of a charge-separated state. For such supramolecular complex, fluorescence and laser flash studies indicate that the main deactivation process is energy transfer from the singlet Zn(II)TTP excited-state to the pyridine-substituted SWCNT with concomitant emission from the carbon nanotube.

Pyridine-functionalized MWCNTs have also been complexed to Ru(II)Pcs via metal–ligand interaction, repeating the Ru(II)Pc/MWCNT deposition process until the desired number of layers was achieved [97]. This layer-by-layer method allowed to prepare self-assembled films of Ru(II)Pc/MWCNT on both modified silicon and ITO substrates, which were characterized using UV/vis absorption spectroscopy, scanning electron microscopy, and electrochemistry.

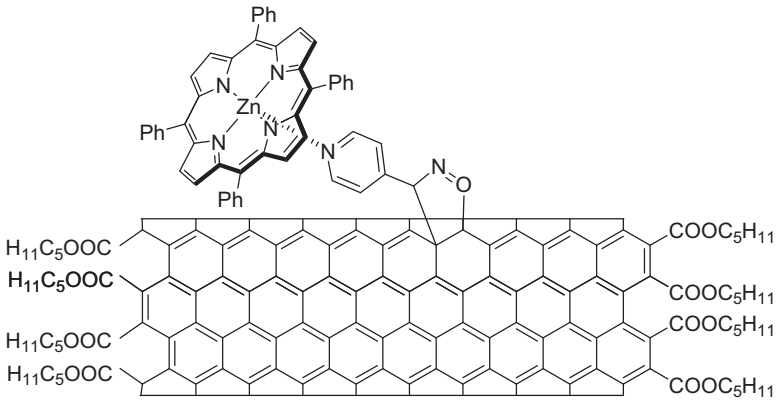

Fig. 39. Structure of the Zn(II)TTP/pyridine-functionalized SWCNT ensemble [96].

The photovoltaic properties of the Ru(II)Pc/MWCNT ensemble deposited on modified ITO substrates were studied showing that, under illumination, (i) the layer-by-layer, self-assembled films gave rise to an efficient photoinduced CT process and (ii) as the number of bilayers was increased, the photocurrent increased reaching a maximum value at nine bilayers (i.e., ~300 nA/cm^2).

5. Porphyrin- and phthalocyanine/graphene supramolecular systems

More recently, graphene, a single atom-thick sheet of carbon and probably the most researched new material of recent times [10], and graphene derivatives have started to be used for the preparation of supramolecular ensembles in conjunction with Pors or Pcs.

The first, and so far only, example of a Pc-based system (**59**, Fig. 37) able to "interact" with graphene via supramolecular interactions has been recently reported [98]. Such study demonstrated that pure, NG was exfoliated in a THF solution of oligomer **59** when subjected to a series of ultrasonication/centrifugation cycles. Absorption studies carried out on the supernatant material showed a significant broadening and red-shift of the Pc's absorption features of the oligomer from 675 to 707 nm, which suggest a strong electronic coupling between the Pc units and graphene. Interestingly, the exfoliated NG/**59** ensemble can be disassembled by addition of Triton X-100 which replaces **59** from the graphene surface, thus restoring the original absorption of the Pc oligomer. The occurrence of supramolecular interactions between the Pc units of **59** and exfoliated NG was also inferred by fluorescence studies carried out on oligomer **59** and exfoliated NG/**59** hybrid, which showed, for the latter system, a considerable quenching of the Pc fluorescence (i.e., 60%) compared to pure **59**. Further proofs of the exfoliation ability of oligomer **59** toward NG came from (i) TEM investigation, which showed for the exfoliated NG/**59** hybrid system images typical of mono/few layers of graphene (Fig. 40), and (ii) resonant and non-resonant Raman studies, which showed changes in the D, 2D, and G-bands of the hybrid system typical of graphene exfoliation.

Finally, insights into the photoinduced dynamics (i.e., electron transfer vs. energy transfer) of the exfoliated NG/**59** ensemble were obtained by using time-resolved measurements. Femtosecond flash photolysis experiments exciting the ensemble either at 387 (where both "free" and "bound" oligomer **59** absorb) or 700 nm (where only the "bound" oligomer species of the exfoliated NG/**59** hybrid absorbs) the formation of the Pc radical cation and exfoliated, NG radical anion species, at 840 and 1290 nm, respectively. The formation of these charged species suggests an electron transfer process from the photoexcited Zn(II)Pc, the electron donor, to the exfoliated graphene, the electron acceptor, giving rise to an electron transfer photoproduct that has a lifetime of 360 ps. The potential use of the exfoliated NG/**59** hybrid in solar energy conversion schemes has also been investigated by manufacturing a solar cell prototype, although low photocurrents were recorded for the unoptimized device.

Recent reports have also appeared describing the supramolecular interactions of Pors with graphene or graphene derivatives. For example, the complexation of a free-base Por bearing four cationic methylpyridinium moieties with negatively charged, CCG sheets by simply mixing diluted aqueous solutions of both components have been demonstrated [99]. The formation of the resulting supramolecular ensemble was inferred by the large bathochromic shift (from 421 to 458 nm) of the Por Soret band. This red-shift was attributed to the flattening of the tetracationic Por macrocycle induced by CCG through a combination of electrostatic and π–π stacking cooperative interactions. Furthermore, it was demonstrated that the incorporation of Cd^{2+} ions into the H_2Por macrocycles was greatly accelerated (from 20 h to 8 min) under ambient conditions by the introduction of CCG sheets, thus paving the way for the utilization of such Por^{4+}/CCG supramolecular ensemble as an optical probe for the rapid and selective detection of Cd^{2+} ions in aqueous media.

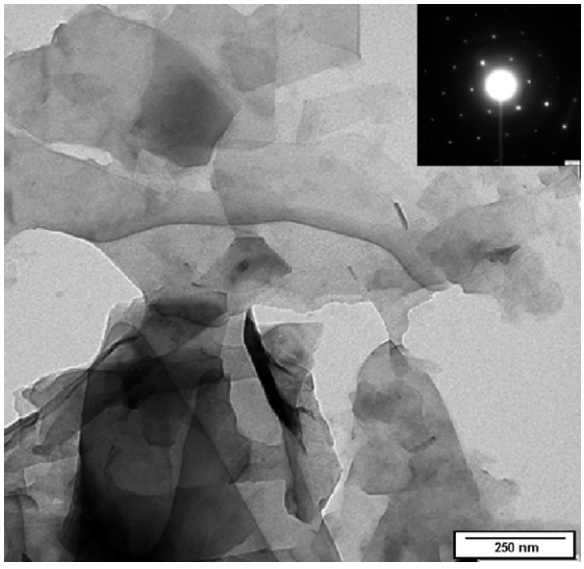

Fig. 40. TEM image and selected area electron diffractogram (inset) of exfoliated NG/59 drop-casted onto a carbon-coated copper grid.
The image is reprinted with permission from Ref. [98].

More recently, a tricomponent, supramolecular ensemble composed of an acid-substituted Zn(II)Por, ZnONPs and RGO has been reported and its photovoltaic properties studied [100]. The organic and inorganic components are sequentially organized on the electrode by (i) anchoring the ZnONPs on the two-dimensional, RGO scaffold leading to a ZnONPs/RGO ensemble, (ii) adsorption of the Zn(II)Pors on the ZnONPs/RGO ensemble and finally (iii) electrophoretic deposition of the resulting organic/inorganic composites onto sintered SnO_2 nanoparticles on a fluorine-doped tin oxide electrode. The resulting electrophoretically deposited films exhibited remarkably high photocurrent generation (IPCE = 70% at 440 nm) compared to the reference devices without ZnONPs and RGO sheets. This improvement in the photogeneration for the tricomponent ensemble could be explained considering a significant contribution to the photocurrent from the additional pathway(s) offered by ZnONPs and/or RGO to the electron injection occurring from the singlet excited Zn(II)Por to the conduction band of the SnO_2.

6. Conclusions

During the past few decades, significant effort has been directed toward the preparation and study of synthetic model compounds that mimic the multifaceted functions of natural photosynthetic systems, ranging from light-harvesting to CT and photoconversion. In this context, D–A materials assembled by using supramolecular interactions and comprising Pors and/or Pcs as donor moieties, and carbon nanostructures like C_{60} fullerene, SWCNTs or graphene as acceptor materials are among the most interesting and investigated systems.

Pors and their synthetic analogues Pcs are compounds which present, beside a rich redox chemistry, an intense optical absorption in the red/NIR of the solar spectrum, thus representing perfect light-harvesting systems and ideal components for the construction of artificial photosynthetic systems. On the other hand, carbon nanostructures like C_{60} fullerene, SWCNTs or graphene possess unique electron accepting features which render them perfect molecular partners for photo- and electroactive systems such as Pors or Pcs. Finally, the use of supramolecular interactions as strategy for the assembly of D–A ensembles based on Pors/Pcs and carbon nanostructures clearly shows significant benefits. The adequate functionalization of the donor and the acceptor units with appropriate, and complementary, recognition elements (e.g., crown ethers and cations, ligand moieties and metal centers, π–π interactions, etc.), in fact, allows the reversible assembly on these components giving rise to supramolecular, D–A systems by using an easy and convergent, "mix and match" strategy. Moreover, this assembly strategy based on noncovalent interactions allow, having prepared a series of donor and acceptor compounds bearing complementary recognition motifs, to realize multiple combinations of these two moieties, thus, being able to generate large libraries of D–A ensembles.

Photophysical studies on several of these Por- and Pc/carbon nanostructure ensembles have showed the occurrence, in the majority of the cases, of efficient PET processes, leading, for some of these systems, to charge-separated lifetimes much longer than analogous, covalently-linked conjugates. Moreover, for such supramolecular, D–A systems, even subtle changes in some structural (i.e., structural variations carried out at the recognition element itself or in its close proximity) and/or physical (i.e., solvent used, temperature, etc.) parameters often have a strong influence on the stability of these self-assembled architectures, which lead to significant changes on the photophysical properties of these ensembles.

Although important advances have been made toward the preparation of self-assembled, D–A Por- and Pc/carbon nanostructure systems and in the study of their photophysical properties, more work is needed in order to precisely predict and control the physicochemical properties of the resulting noncovalent ensembles, in solution as well as in condensed phases. In this sense, future challenges for this field include not only a better comprehension of the photophysical features of these D–A systems, but also, and probably more importantly, the implementation of these supramolecular architectures into efficient, photovoltaic devices, where much work remains to be done. In this context, the search for new D–A systems with appropriate HOMO–LUMO levels for maximizing charges injection into the electrodes will definitely be beneficial. At the same time, the possibility to control/promote the long-range order of these systems over large length scales should also be strongly pursued, since the order of both, acceptor and donor active components within the photovoltaic devices is a key issue for achieving high charges mobilities, thus, representing an important point for the development of efficient organic solid state solar cells.

The challenges and opportunities that rest on these systems are clearly enormous and it should attract the efforts of many researchers in this important area.

Acknowledgments

This work has been supported by the Spanish MICINN (CTQ2011-24187/BQU and CONSOLIDER INGENIO 2010, CSD2007-00010 and PLE2009-0070) and the Comunidad de Madrid (MADRISOLAR-2, S2009/PPQ/1533). We thank the Spanish MICINN for a "Ramón y Cajal" contract (G.B.) and the Universidad Autónoma de Madrid (UAM) for a predoctoral fellowship (O.T.). We also thank the UAM for providing excellent research conditions and infrastructure, as well as to all students, co-workers, and senior researchers who perform exciting research in this area in our group.

References

[1] K. Kadish, K.M. Smith, R. Guilard (Eds.), Handbook of Porphyrin Science, Vols. 10–20, World Scientific Press, 2010–2012.
[2] (a) G. de la Torre, C.G. Claessens, T. Torres, Chem. Commun. (2007) 2000;
(b) G. de la Torre, G. Bottari, U. Hahn, T. Torres, Struct. Bond. 135 (2010) 1.
[3] D.M. Guldi, N. Martin (Eds.), Carbon Nanotubes and Related Structures: Synthesis, Characterization, Functionalization, and Applications, Wiley, 2010.
[4] Y. Rio, M.S. Rodríguez-Morgade, T. Torres, Org. Biomol. Chem. 6 (2008) 1877.
[5] (a) M.V. Martínez-Díaz, G. de la Torre, T. Torres, Chem. Commun. 46 (2010) 7090;
(b) M.G. Walter, A.B. Rudine, C.C. Wamser, J. Porphyrins Phthalocyanines 14 (2010) 759.
[6] (a) M.R. Wasielewski, Chem. Rev. 92 (1992) 435;
(b) A. Osuka, N. Mataga, T. Okada, Pure Appl. Chem. 69 (1997) 797;
(c) M.R. Wasielewski, J. Org. Chem. 71 (2006) 5051.
[7] The total reorganization energy λ is composed of two components, a solvent-independent part λ_v, which accounts for the different nuclear configurations of the initial and final states in a transformation leading to a charge-separated species product, and a solvent-dependent part λ_s. C_{60} fullerene has a small λ value compared to two-dimensional electron acceptors, which in general have less rigid structures. In C_{60}, the λ_v contribution is very small ($\lambda_v \sim 0.06$ eV) due to the structural similarity between C_{60} in the ground, reduced and excited-state, stemming from the structural rigidity of this spherical carbon nanostructure. It is also believed that, in C_{60}, the solvent-dependent term λ_s is small, since the adjustment of the solvent environment to the newly-formed, excited or reduced state o requires little energy, due to the symmetrical shape and large size of the fullerene molecule. The total reorganization energy λ, which appears in the classical Marcus treatment of electron transfer reactions, strongly influences the rate of the electron transfer process. The Marcus theory predicts that the dependence of electron transfer rates on the free energy changes of the reaction ($-\Delta_{GET^\circ}$) is a parabolic curve. In the 'normal region' of the Marcus parabola, the theory predicts an increase in the electron transfer rate with increase of the thermodynamic driving force (i.e., $-\Delta_{GET^\circ} < \lambda$). The rate of the electron transfer then reaches a maximum when the driving force equals the overall reorganization energy (i.e., $-\Delta_{GET^\circ} \sim \lambda$). Beyond this thermodynamic maximum, the process becomes exergonic, with the electron transfer rate decreasing while increasing the free energy changes ('inverted region') (i.e., $-\Delta_{GET^\circ} > \lambda$). In principle, systems with small λ values such as C_{60} fullerene allow one to reach the maximum of the Marcus parabola (which represents the point in

which the electron transfer rate is at its maximum) at small $-\Delta_{GET^\circ}$ values and, in turn, to shift the charge-recombination rate constant deeply into the Marcus 'inverted region', thus retarding the undesired back-electron transfer process.

[8] (a) N. Martin, L. Sanchez, B. Illescas, I. Perez, Chem. Rev. 98 (1998) 2527;
(b) D.M. Guldi, M. Prato, Acc. Chem. Res. 33 (2000) 695;
(c) S. Fukuzumi, D.M. Guldi, in: V. Balzani (Ed.), Electron Transfer in Chemistry, Vol. 2, Wiley-VCH, New York, 2001, p. 270;
(d) F. Langa, J.-F. Nierengarten (Eds.), Fullerenes: Principles and Applications, Nanoscience and Nanotechnology Series, The Royal Society of Chemistry, Cambridge, U.K., 2007;
(e) J.L. Delgado, M.A. Herranz, N. Martin, J. Mater. Chem. 18 (2008) 1417;
(f) D.M. Guldi, B.M. Illescas, C.M. Atienza, M. Wielopolski, N. Martin, Chem. Soc. Rev. 38 (2009) 1587.

[9] (a) S. Reich, C. Thomsen, J. Maultzsh (Eds.), Carbon Nanotubes: Basic Concepts and Physical Properties, VCH, Weinheim, Germany, 2004;
(b) D. Tasis, N. Tagmatarchis, A. Bianco, M. Prato, Chem. Rev. 106 (2006) 1105;
(c) V. Sgobba, D.M. Guldi, J. Mater. Chem. 18 (2008) 153;
(d) V. Sgobba, D.M. Guldi, Chem. Soc. Rev. 38 (2009) 165;
(e) T. Akasaka, F. Wudl, S. Nagase (Eds.), Chemistry of Nanocarbons, Wiley, 2010.

[10] A.K. Geim, K.S. Novoselov, Nat. Mater. 6 (2007) 183.

[11] B. Luo, S. Liu, L. Zhi, Small 8 (2012) 630.

[12] (a) D.M. Guldi, Chem. Soc. Rev. 31 (2002) 22;
(b) M.E. El-Khouly, O. Ito, P.M. Smith, F. D'Souza, J. Photochem. Photobiol. C 5 (2004) 79;
(c) F. D'Souza, O. Ito, Coord. Chem. Rev. 249 (2005) 1410;
(d) R. Chitta, F. D'Souza, J. Mater. Chem. 18 (2008) 1440;
(e) F. D'Souza, O. Ito, Chem. Commun. 33 (2009) 4913.

[13] (a) G. Bottari, G. de la Torre, D.M. Guldi, T. Torres, Chem. Rev. 110 (2010) 6768;
(b) D. Gonzalez-Rodriguez, G. Bottari, J. Porphyrins Phthalocyanines 13 (2009) 624.

[14] (a) P.D.W. Boyd, C.A. Reed, Acc. Chem. Res. 38 (2005) 235;
(b) K. Tashiro, T. Aida, Chem. Soc. Rev. 36 (2007) 189;
(c) D. Canevet, E.M. Pérez, N. Martín, Angew. Chem. Int. Ed. 50 (2011) 9248.

[15] T. Torres, A. Gouloumis, D. Sanchez-Garcia, J. Jayawickramarajah, W. Seitz, D.M. Guldi, J.L. Sessler, Chem. Commun. (2007) 292.

[16] J.L. Sessler, J. Jayawickramarajah, A. Gouloumis, T. Torres, D.M. Guldi, S. Maldonado, K.J. Stevenson, Chem. Commun. (2005) 1892.

[17] J.L. Sessler, J. Jayawickramarajah, A. Gouloumis, G.D. Pantos, T. Torres, D.M. Guldi, Tetrahedron 62 (2006) 2123.

[18] S. Gadde, D.M.S. Islam, C.A. Wijesinghe, N.K. Subbaiyan, M.E. Zandler, Y. Araki, O. Ito, F. D'Souza, J. Phys. Chem. C 111 (2007) 12500.

[19] L. Sanchez, M. Sierra, N. Martin, A.J. Myles, T.J. Dale, J. Rebek Jr., W. Seitz, D.M. Guldi, Angew. Chem. Int. Ed. 45 (2006) 4637.

[20] F. D'Souza, G.M. Venukadasula, K.-i. Yamanaka, N.K. Subbaiyan, M.E. Zandler, O. Ito, Org. Biomol. Chem. 7 (2009) 1076.

[21] F. Wessendorf, J.-F. Gnichwitz, G.H. Sarova, K. Hager, U. Hartnagel, D.M. Guldi, A. Hirsch, J. Am. Chem. Soc. 129 (2007) 16057.

[22] F. Wessendorf, B. Grimm, D.M. Guldi, A. Hirsch, J. Am. Chem. Soc. 132 (2010) 10786.

[23] Charge-separation and charge-recombination processes occur with kinetics which are defined by the electron transfer rate constant: $k_{ET} = k_0\, e^{-\beta rDA}$, where k_0 is a kinetic prefactor, rDA represents the D–A distance, and the factor β, which depends primarily on the nature of the bridge, often used to estimate the wire-like behavior of the bridging unit connecting the donor and acceptor moieties. The smaller this factor β, the longer is the distance over which charge can be conducted efficiently. Typical values for β range between 1.0 and 1.4 $Å^{-1}$ for proteins, and between 0.01 and 0.04 $Å^{-1}$ for highly efficient π-conjugated bridges.

[24] B. Grimm, J. Schornbaum, H. Jasch, O. Trukhina, F. Wessendorf, A. Hirsch, T. Torres, D.M. Guldi, Proc. Natl. Acad. Sci. U.S.A., doi:10.1073/pnas.1113753109, in press.

[25] M.V. Martinez-Diaz, N.S. Fender, M.S. Rodriguez-Morgade, M. Gomez-Lopez, F. Diederich, L. Echegoyen, J.F. Stoddart, T. Torres, J. Mater. Chem. 12 (2002) 2095.

[26] D.M. Guldi, J. Ramey, M.V. Martinez-Diaz, A. de la Escosura, T. Torres, T. Da Ros, M. Prato, Chem. Commun. (2002) 2774.

[27] N. Solladie, M.E. Walther, M. Gross, T.M. Figueira Duarte, C. Bourgogne, J.-F. Nierengarten, Chem. Commun. (2003) 2412.

[28] A.S.D. Sandanayaka, Y. Araki, O. Ito, R. Chitta, S. Gadde, F. D'Souza, Chem. Commun. (2006) 4327.

[29] F. D'Souza, R. Chitta, S. Gadde, M.E. Zandler, A.L. McCarty, A.S.D. Sandanayaka, Y. Araki, O. Ito, Chem. Eur. J. 11 (2005) 4416.

[30] F. D'Souza, R. Chitta, S. Gadde, M.E. Zandler, A.S.D. Sandanayaka, Y. Araki, O. Ito, Chem. Commun. (2005) 1279.

[31] F. D'Souza, R. Chitta, S. Gadde, A.L. McCarty, P.A. Karr, M.E. Zandler, A.S.D. Sandanayaka, Y. Araki, O. Ito, J. Phys. Chem. B 110 (2006) 5905.

[32] F. D'Souza, E. Maligaspe, K. Ohkubo, M.E. Zandler, N.K. Subbaiyan, S. Fukuzumi, J. Am. Chem. Soc. 131 (2009) 8787.

[33] F. D'Souza, R. Chitta, S. Gadde, L.M. Rogers, P.A. Karr, M.E. Zandler, A.S.D. Sandanayaka, Y. Araki, O. Ito, Chem. Eur. J. 13 (2007) 916.

[34] F. D'Souza, E. Maligaspe, A.S.D. Sandanayaka, N.K. Subbaiyan, P.A. Karr, T. Hasobe, O. Ito, J. Phys. Chem. A 114 (2010) 10951.

[35] F. D'Souza, G.R. Deviprasad, M.S. Rahman, J.P. Choi, Inorg. Chem. 38 (1999) 2157.

[36] F. D'Souza, G.R. Deviprasad, M.E. Zandler, V.T. Hoang, A. Klykov, M. VanStipdonk, A. Perera, M.E. El-Khouly, M. Fujitsuka, O. Ito, J. Phys. Chem. A 106 (2002) 3243.

[37] T. Da Ros, M. Prato, D.M. Guldi, M. Ruzzi, L. Pasimeni, Chem. Eur. J. 7 (2001) 816.

[38] (a) S.R. Wilson, S. MacMahon, F.T. Tat, P.D. Jarowski, D.I. Schuster, Chem. Commun. (2003) 226;
(b) F.T. Tat, Z. Zhou, S. MacMahon, F. Song, A.L. Rheingold, L. Echegoyen, D.I. Schuster, S.R. Wilson, J. Org. Chem. 69 (2004) 4602;
(c) A. Regev, T. Galili, H. Levanon, D.I. Schuster, J. Phys. Chem. A 110 (2006) 8593.

[39] N. Armaroli, F. Diederich, L. Echegoyen, T. Habicher, L. Flamigni, G. Marconi, J.-F. Nierengarten, New J. Chem. 23 (1999) 77.

[40] M.E. El-Khouly, L.M. Rogers, M.E. Zandler, G. Suresh, M. Fujitsuka, O. Ito, F. D'Souza, ChemPhysChem 4 (2003) 474.

[41] M.E. El-Khouly, Y. Araki, O. Ito, S. Gadde, M.E. Zandler, F. D'Souza, J. Porphyrins Phthalocyanines 10 (2006) 1156.

[42] M.E. El-Khouly, M.E. Zandler, Y. Araki, O. Ito, J. Porphyrins Phthalocyanines 9 (2005) 698.

[43] F. D'Souza, P.M. Smith, S. Gadde, A.L. McCarty, M.J. Kullman, M.E. Zandler, M. Itou, Y. Araki, O. Ito, J. Phys. Chem. B 108 (2004) 11333.

[44] F. D'Souza, S. Gadde, M.E. Zandler, M. Itou, Y. Araki, O. Ito, Chem. Commun. (2004) 2276.

[45] M.S. Rodriguez-Morgade, M.E. Plonska-Brzezinska, A.J. Athans, E. Carbonell, G. de Miguel, D.M. Guldi, L. Echegoyen, T. Torres, J. Am. Chem. Soc. 131 (2009) 10484.

[46] A. Mateo-Alonso, C. Ehli, D.M. Guldi, M. Prato, J. Am. Chem. Soc. 130 (2008) 14938.

[47] F. D'Souza, M.E. El-Khouly, S. Gadde, A.L. McCarty, P.A. Karr, M.E. Zandler, Y. Araki, O. Ito, J. Phys. Chem. B 109 (2005) 10107.

[48] B. Ballesteros, G. de la Torre, T. Torres, G.L. Hug, G.M.A. Rahman, D.M. Guldi, Tetrahedron 62 (2006) 2097.

[49] D.M. Guldi, C. Luo, M. Prato, A. Troisi, F. Zerbetto, M. Scheloske, E. Dietel, W. Bauer, A. Hirsch, J. Am. Chem. Soc. 123 (2001) 9166.

[50] F. Hauke, A. Swartz, D.M. Guldi, A. Hirsch, J. Mater. Chem. 12 (2002) 2088.

[51] A.M.V.M. Pereira, A.R.M. Soares, A. Hausmann, M.G.P.M.S. Neves, A.C. Tome, A.M.S. Silva, J.A.S. Cavaleiro, D.M. Guldi, T. Torres, Phys. Chem. Chem. Phys. 13 (2011) 11858.

[52] A.M.V.M. Pereira, A. Hausmann, J.P.C. Tomé, O. Trukhina, M. Urbani, M.G.P.M.S. Neves, J.A.S. Cavaleiro, D.M. Guldi, T. Torres, Chem. Eur. J. (2012), doi:10.1002/chem.201103776.

[53] D.M. Guldi, C. Luo, T. Da Ros, M. Prato, E. Dietel, A. Hirsch, Chem. Commun. (2000) 375.

[54] F. D'Souza, G.R. Deviprasad, M.E. Zandler, M.E. El-Khouly, M. Fujitsuka, O. Ito, J. Phys. Chem. B 106 (2002) 4952.

[55] F. D'Souza, S. Gadde, A.L. Schumacher, M.E. Zandler, A.S.D. Sandanayaka, Y. Araki, O. Ito, J. Phys. Chem. B 111 (2007) 11123.

[56] F. D'Souza, M.E. El-Khouly, S. Gadde, M.E. Zandler, A.L. McCarty, Y. Araki, O. Ito, Tetrahedron 62 (2006) 1967.

[57] F. D'Souza, P.M. Smith, M.E. Zandler, A.L. McCarty, M. Itou, Y. Araki, O. Ito, J. Am. Chem. Soc. 126 (2004) 7898.

[58] E. Maligaspe, T. Kumpulainen, N.K. Subbaiyan, M.E. Zandler, H. Lemmetyinen, N.V. Tkachenko, F. D'Souza, Phys. Chem. Chem. Phys. 12 (2010) 7434.

[59] Y. Rio, W. Seitz, A. Gouloumis, P. Vázquez, J.L. Sessler, D.M. Guldi, T. Torres, Chem. Eur. J. 16 (2010) 1929.

[60] M.E. El-Khouly, D.K. Ju, K.-Y. Kay, F. D'Souza, S. Fukuzumi, Chem. Eur. J. 16 (2010) 6193.

[61] Y. Terazono, G. Kodis, P.A. Liddell, V. Garg, T.A. Moore, A.L. Moore, D. Gust, J. Phys. Chem. B 113 (2009) 7147.

[62] J.-L. Hou, H.-P. Yi, X.-B. Shao, C. Li, Z.-Q. Wu, X.-K. Jiang, L.-Z. Wu, C.-H. Tung, Z.-T. Li, Angew. Chem. Int. Ed. 46 (2006) 796.

[63] A. Trabolsi, M. Urbani, J.L. Delgado, F. Ajamaa, M. Elhabiri, N. Solladie, J.-F. Nierengarten, A.-M. Albrecht-Gary, New J. Chem. 32 (2008) 159.

[64] S. Fukuzumi, K. Saito, K. Ohkubo, T. Khoury, Y. Kashiwagi, M.A. Absalom, S. Gadde, F. D'Souza, Y. Araki, O. Ito, M.J. Crossley, Chem. Commun. 47 (2011) 7980.

[65] S. Fukuzumi, K. Saito, K. Ohkubo, V. Troiani, H. Qiu, S. Gadde, F. D'Souza, N. Solladie, Phys. Chem. Chem. Phys. 13 (2011) 17019.

[66] (a) R. Koeppe, N.S. Sariciftci, P.A. Troshin, R.N. Lyubovskaya, Appl. Phys. Lett. 87 (2005) 244102/1;
(b) P.A. Troshin, R. Koeppe, A.S. Peregudov, S.M. Peregudova, M. Egginger, R.N. Lyubovskaya, N.S. Sariciftci, Chem. Mater. 19 (2007) 5363.

[67] A. Varotto, C.-Y. Nam, I. Radivojevic, J.P.C. Tomé, J.A.S. Cavaleiro, C.T. Black, C.M. Drain, J. Am. Chem. Soc. 132 (2010) 2552.

[68] N.K. Subbaiyan, I. Obraztsov, C.A. Wijesinghe, K. Tran, W. Kutner, F. D'Souza, J. Phys. Chem. B 113 (2009) 8982.

[69] A. Kira, T. Umeyama, Y. Matano, K. Yoshida, S. Isoda, J.K. Park, D. Kim, H. Imahori, J. Am. Chem. Soc. 131 (2009) 3198.

[70] G. Bottari, J.A. Suanzes, O. Trukhina, T. Torres, J. Phys. Chem. Lett. 2 (2011) 905.

[71] Y.H. Geerts, O. Debever, C. Amato, S. Sergeyev, Beilstein J. Org. Chem. 5 (2009) 49, doi:10.3762/bjoc.5.49.

[72] M. Ince, M.V. Martinez-Diaz, J. Barbera, T. Torres, J. Mater. Chem. 21 (2011) 1531.

[73] H. Hayashi, W. Nihashi, T. Umeyama, Y. Matano, S. Seki, Y. Shimizu, H. Imahori, J. Am. Chem. Soc. 133 (2011) 10736.
[74] A. de la Escosura, M.V. Martinez-Diaz, J. Barbera, T. Torres, J. Org. Chem. 73 (2008) 1475.
[75] D.M. Guldi, A. Gouloumis, P. Vazquez, T. Torres, V. Georgakilas, M. Prato, J. Am. Chem. Soc. 127 (2005) 5811.
[76] V. Georgakilas, F. Pellarini, M. Prato, D.M. Guldi, M. Melle-Franco, F. Zerbetto, Proc. Natl. Acad. Sci. U.S.A. 99 (2002) 5075.
[77] G. Bottari, D. Olea, C. Gomez-Navarro, F. Zamora, J. Gomez-Herrero, T. Torres, Angew. Chem. Int. Ed. 47 (2008) 2026.
[78] G. Bottari, D. Olea, V. Lopez, C. Gomez-Navarro, F. Zamora, J. Gomez-Herrero, T. Torres, Chem. Commun. 46 (2010) 4692.
[79] H. Yamada, H. Imahori, Y. Nishimura, I. Yamazaki, S. Fukuzumi, Adv. Mater. 14 (2002) 892.
[80] H. Yamada, H. Imahori, Y. Nishimura, I. Yamazaki, T.K. Ahn, S.K. Kim, D. Kim, S. Fukuzumi, J. Am. Chem. Soc. 125 (2003) 9129.
[81] R.J. Chen, Y. Zhang, D. Wang, H. Dai, J. Am. Chem. Soc. 123 (2001) 3838.
[82] J. Bartelmess, B. Ballesteros, G. de la Torre, D. Kiessling, S. Campidelli, M. Prato, T. Torres, D.M. Guldi, J. Am. Chem. Soc. 132 (2010) 16202.
[83] S. Klyatskaya, J.R. Galan-Mascaros, L. Bogani, F. Hennrich, M. Kappes, W. Wernsdorfer, M. Ruben, J. Am. Chem. Soc. 131 (2009) 15143.
[84] J. Bartelmess, A.R.M. Soares, M.V. Martinez-Diaz, M.G.P.M.S. Neves, A.C. Tomé, J.A.S. Cavaleiro, T. Torres, D.M. Guldi, Chem. Commun. 47 (2011) 3490.
[85] R. Chitta, A.S.D. Sandanayaka, A.L. Schumacher, L. D'Souza, Y. Araki, O. Ito, F. D'Souza, J. Phys. Chem. C 111 (2007) 6947.
[86] F. D'Souza, A.S.D. Sandanayaka, O. Ito, J. Phys. Chem. Lett. 1 (2010) 2586.
[87] A.S.D. Sandanayaka, R. Chitta, N.K. Subbaiyan, L. D'Souza, O. Ito, F. D'Souza, J. Phys. Chem. C 113 (2009) 13425.
[88] F. D'Souza, R. Chitta, A.S.D. Sandanayaka, N.K. Subbaiyan, L. D'Souza, Y. Araki, O. Ito, Chem. Eur. J. 13 (2007) 8277.
[89] E. Maligaspe, A.S.D. Sandanayaka, T. Hasobe, O. Ito, F. D'Souza, J. Am. Chem. 132 (2010) 8158.
[90] U. Hahn, S. Engmann, C. Oelsner, C. Ehl, D.M. Guldi, T. Torres, J. Am. Chem. Soc. 132 (2010) 6392.
[91] J. Bartelmess, C. Ehli, J.-J. Cid, M. García-Iglesias, P. Vázquez, T. Torres, D.M. Guldi, Chem. Sci. 2 (2011) 652.
[92] J. Bartelmess, C. Ehli, J.-J. Cid, M. Garcia-Iglesias, P. Vazquez, T. Torres, D.M. Guldi, J. Mater. Chem. 21 (2011) 8014.
[93] F. Cheng, A. Adronov, Chem. Eur. J. 12 (2006) 5053.
[94] F. Cheng, S. Zhang, A. Adronov, L. Echegoyen, F. Diederich, Chem. Eur. J. 12 (2006) 6062.
[95] H. Li, B. Zhou, Y. Lin, L. Gu, W. Wang, K.A.S. Fernando, S. Kumar, L.F. Allard, Y.-P. Sun, J. Am. Chem. Soc. 126 (2004) 1014.
[96] M. Alvaro, P. Atienzar, P. De la Cruz, J.L. Delgado, V. Troiani, H. Garcia, F. Langa, A. Palkar, L. Echegoyen, J. Am. Chem. Soc. 128 (2006) 6626.
[97] W. Zhao, B. Tong, J. Shi, Y. Pan, J. Shen, J. Zhi, W.K. Chan, Y. Dong, Langmuir 26 (2010) 16084.
[98] J. Malig, N. Jux, D. Kiessling, J.-J. Cid, P. Vázquez, T. Torres, D.M. Guldi, Angew. Chem. Int. Ed. 50 (2011) 3561.
[99] Y. Xu, L. Zhao, H. Bai, W. Hong, C. Li, G. Shi, J. Am. Chem. Soc. 131 (2009) 13490.
[100] H. Hayashi, I.V. Lightcap, M. Tsujimoto, M. Takano, T. Umeyama, P.V. Kamat, H. Imahori, J. Am. Chem. Soc. 133 (2011) 76.